Composite Structures 279 (2022) 114828

Contents lists available at ScienceDirect

Composite Structures

journal homepage: www.elsevier.com/locate/compstruct

Detailed experimental validation and benchmarking of six models for longitudinal tensile failure of unidirectional composites

C. Breite [a], A. Melnikov [a], A. Turon [b], A.B. de Morais [c], C. Le Bourlot [d], E. Maire [d], E. Schöberl [e], F. Otero [f], F. Mesquita [a], I. Sinclair [e], J. Costa [b], J.A. Mayugo [b], J.M. Guerrero [b], L. Gorbatikh [a], L. N. McCartney [g], M. Hajikazemi [h,i], M. Mehdikhani [a], M.N. Mavrogordato [e], P.P. Camanho [f,j], R. Tavares [f,j], S.M. Spearing [e], S.V. Lomov [a], S. Pimenta [k], W. Van Paepegem [h], Y. Swolfs [a,*]

[a] Department of Materials Engineering, KU Leuven, Kasteelpark Arenberg 44 box 2450, 3001 Leuven, Belgium
[b] AMADE, Polytechnic School, University of Girona, Campus Montilivi s/n, E-17003 Girona, Spain
[c] Department of Mechanical Engineering, RISCO Research Unit, University of Aveiro, Campus Santiago, 3810-193 Aveiro, Portugal
[d] Universite de Lyon, INSA-Lyon, MATEIS, CNRS UMR5510, F-69621 Villeurbanne, France
[e] Engineering Materials, Faculty of Engineering and Physical Sciences, University of Southampton, Southampton SO17 1BJ, UK
[f] INEGI, Rua Dr. Roberto Frias 400, 4200-465 Porto, Portugal
[g] Department of Engineering, Materials & Electrical Science, National Physical Laboratory, Teddington, Middlesex TW11 0LW, UK
[h] Department of Materials, Textiles and Chemical Engineering, Faculty of Engineering and Architecture, Ghent University, Technologiepark Zwijnaarde 46, Ghent, Belgium
[i] Dutch Polymer Institute (DPI), P.O. Box 902, 5600 AX Eindhoven, The Netherlands
[j] DEMec, Faculdade de Engenharia, Universidade do Porto, Rua Dr. Roberto Frias, 4200-465 Porto, Portugal
[k] meComposites, Department of Mechanical Engineering, Imperial College London, South Kensington Campus, London SW7 2AZ, UK

ARTICLE INFO

Keywords:
Polymer-matrix composites (PMCs)
Fracture
Material modelling
X-ray computed tomography

ABSTRACT

Longitudinal tensile failure of unidirectional fibre-reinforced composites remains difficult to predict accurately. The key underlying mechanism is the tensile failure of individual fibres. This paper objectively measured the relevant input data and performed a detailed experimental validation of blind predictions of six state-of-the-art models using high-resolution *in-situ* synchrotron radiation computed tomography (SRCT) measurements on two carbon fibre/epoxy composites. Models without major conservative assumptions regarding stress redistributions around fibre breaks significantly overpredicted failure strains and strengths, but predictions of models with at least one such assumption were in better agreement for those properties. Moreover, all models failed to predict fibre break (and cluster) development accurately, suggesting that it is vital to improve experimental methods to characterise accurately the *in-situ* strength distribution of fibres within the composites. As a result of detailed measurements of all required input parameters and advanced SRCT experiments, this paper establishes a benchmark for future research on longitudinal tensile failure.

1. Introduction

Longitudinal tensile failure of unidirectional plies is a crucial damage mode in fibre-reinforced composite laminates, as it often governs final failure. This mode has historically received considerable attention, both in terms of rule-of-mixtures and mean-field type of predictions [1] and in terms of fibre break models [2]. The basic mechanisms are qualitatively well understood [2,3]. Firstly, fibre strength varies significantly, which causes the weakest fibre to break under relatively low remote strains. Secondly, a broken fibre transfers load to the surrounding fibres, but further away from the break, it recovers that load through shear stress transfer via the interface and matrix. The relative stress increase in the intact fibres compared to the nominal stress is often referred to as the stress concentration factor (SCF). While these two basic mechanisms are generally accepted to be the basis for longitudinal tensile failure, there are still lively ongoing discussions as to the best way to capture them in models.

The unimodal Weibull distribution has often been used to model the stochastic nature of fibre strength [2], although many authors have suggested alternative versions, such as the bimodal Weibull distribution

* Corresponding author.
E-mail address: yentl.swolfs@kuleuven.be (Y. Swolfs).

https://doi.org/10.1016/j.compstruct.2021.114828
Received 26 March 2021; Received in revised form 7 September 2021; Accepted 12 October 2021
Available online 16 October 2021
0263-8223/© 2021 Elsevier Ltd. All rights reserved.

[4], the power law-accelerated [5–8] or the Weibull-of-Weibull distribution [9]. Some authors have emphasised the importance of testing a sufficient number of fibres to be able to determine the Weibull parameters accurately [10,11]. Other authors identified experimental issues in single fibre tensile testing, such as fibre alignment [12–14], fibre diameter variation [12,14] and stress concentrations associated to fibre gripping [15]. Other hypotheses have also been raised, such as whether the strength of fibres embedded in a resin is different from the one measured in bare fibre tests, but these remain unproven [16].

The stress redistribution around fibre breaks was first modelled by Hedgepeth [17] through shear-lag theory in a 2D formulation. Later, this theory was extended to a 3D formulation [18–20], with researchers using Green's functions [21], finite element (FE) models [22–30] and spring element models [31–34]. There are, however, significant differences between these approaches:

- The assumptions regarding matrix behaviour vary from elastic [17–19,22–24,31,32] to perfectly plastic [35], linear elastic-perfect plastic [23,29,32,33], viscoelastic [28] and elastoplastic [25–27,34]. The actual behaviour of typical thermosets is assumed to be even more complex [36].
- Some models consider the possibility of fibre–matrix debonding [37,38], whereas others do not.
- Some approaches capture dynamic stress concentrations due to the sudden brittle nature of fibre failure [17,32,39], but most do not.
- Initial models focused on regular fibre packings [18,19,21–23,26–29,31,34], but in recent years random packings have become more commonly implemented [24,25,32,33,39,40] due to increasing computational power and the popularity of numerical models.

These different approaches can lead to significant differences in the predicted stress redistribution [23,24,32]. When the approaches are different, objective comparisons become challenging.

Initial experimental work aimed at validating FE models used micro-Raman spectroscopy to measure strains in fibres [26,27,41]. FE models with an elastoplastic matrix [26,27] and shear-lag predictions with an elastic matrix [41] achieved good agreement with micro-Raman strain profiles. Raman spectroscopy is necessarily restricted to imaging fibres at specimen surfaces, and, in most cases, to single fibre specimens or specimens with low volume fractions. In recent years, the focus of experimental validations has, therefore, shifted towards the use of synchrotron radiation computed tomography (SRCT) [16,42–50]. SRCT allows three-dimensional *in-situ* observation of fibres within the bulk of composites, albeit with small imaging volumes (~1 mm^3) at the required resolution. While methods to measure strain profiles are being developed [49,51–53], the research has primarily focused on monitoring the development of fibre breaks and clusters thereof. Direct comparisons with model predictions have led to useful insights [16,32,42,43,54], but the models still need improvements in order to predict the coplanarity of the clusters [16] and size of the clusters [16,32,42,54]. These studies were, however, all based on just one specimen. Although those specimens contained about 5500 fibres and break densities of 400–500/mm^3, this nonetheless calls into question the repeatability of the experiments. Further questions arise about the accuracy of the Weibull fibre strength distribution used in those studies, and the possibility of additional fibre breaks due to stress relaxation caused by the hold-at-displacement method employed [16,42,43].

There is, hence, a clear need for a detailed experimental study of longitudinal tensile failure as well as a rigorous comparison of available models with the key input parameters objectively measured. This paper, therefore, presents steps towards a benchmarking exercise for six state-of-the-art longitudinal tensile failure models, involving a detailed comparison of predictions with experiments. The entire study is performed for two types of carbon fibre/epoxy composites. Two SRCT specimens of each composite were tested to obtain some indication of their repeatability. In addition, macroscale tensile tests were performed to provide a more reliable baseline failure strain for both composites. In contrast with previous experimental validation studies based on SRCT [16,42,43,54], this is the first time that: (1) the Weibull strength distribution and matrix properties, which are needed as input for the models, are characterised through extensive testing and independently rather than being estimated from the literature and data sheets, (2) more than one material set is used, (3) the repeatability of the SRCT experiments is analysed, and (4) the SRCT data is accompanied by macroscale tensile test results.

2. Materials and methods

2.1. Materials

Carbon fibre/epoxy prepregs with Grafil 34-700WD-24 K-1.4%A carbon fibres (Mitsubishi Chemical) and proprietary 736LT resin were sourced from North Thin Ply Technology (Switzerland). These prepregs had a fibre areal density of approximately 38 g/m^2 and a cured ply thickness of around 44 μm. A 34–700 bobbin and the neat resin that was used to make these prepregs were also supplied. T700SC-12 K-50C carbon fibre bobbins and SiPreg SR8500-KTA315 epoxy prepregging resin were sourced from Toray Europe (France) and Sicomin (France), respectively. Prepregs were manufactured with this fibre type and resin on the hot melt drum winder at KU Leuven [52], yielding prepregs with a fibre areal density of about 172 g/m^2 and a cured ply thickness of 191 μm. These materials are correspondingly referred hereafter to as "34–700" and "T700SC".

Prepregs with HYBON-2026 E-glass fibres and 736LT epoxy resin were also sourced from North Thin Ply Technology. They had a nominal fibre areal density of 50 g/m^2, an average cured ply thickness of 34 μm and a fibre volume fraction of 58%. Finally, S-2 SCG75 glass fibre prepregs with a 913 epoxy matrix were sourced from Hexcel (UK). They had a nominal fibre areal density of 190 g/m^2, an average cured ply thickness of 150 μm and a fibre volume fraction of 60%.

2.2. Manufacturing

Two types of specimens were manufactured, and they are designated as microscale and macroscale specimens. Even though the focus is on unidirectional composites, cross-ply laminates were used to enable efficient load introduction of the microscale specimens inside the SRCT load rig. This is in line with previous SRCT studies [16,43–45,48,55–57]. The effect of the 90° plies was monitored, but found not to affect the measured 0° fibre break development (this will be explained in section 2.4). $\left[90_4^C/0_4^C\right]_s$ and $\left[90^C/0^C\right]_s$ layups were manufactured for the microscale 34–700 and T700SC cases, respectively. $\left[0_{16}^{EG}/90_4^C/0_4^C\right]_s$ and $\left[0_5^{SG}/90^C/0^C\right]_s$ hybrid laminates were co-cured for the macroscale 34–700 and T700SC specimens, respectively. The superscripts C, EG and SG stand for carbon, E-glass and S-glass layers, respectively. The glass layers eliminate stress concentrations on the carbon layers at the grips and thus enable failure in the gauge section [58,59].

After manually stacking 300 × 300 mm^2 laminates, they were cured in KU Leuven's autoclave according to the manufacturer's recommendations [60,61]. For the 34–700 layups, the temperature was first increased from room temperature to 70 °C at 2 °C/min and held constant for 60 min. Next, the temperature was increased to 120 °C at 1.4 °C/min and held constant for 45 min. The autoclave was then cooled down back to room temperature at 1.4 °C/min and opened when the temperature was below 40 °C. A vacuum pressure of −0.7 bar was applied during the whole cycle. The overpressure of 5 bar was applied from the moment 70 °C was reached until the end of the cycle. For the T700SC layups, the heating rates were 2.8 and 1.4 °C/min, respectively, and the dwell time at 120 °C was 90 rather than 45 min.

2.3. Macroscale composite tensile testing

Rectangular, parallel-sided specimens without a notch were cut from the panels using a water-cooled diamond saw. Tensile tests were performed according to ASTM D3039 using a Zwick Z100 universal testing machine, equipped with a 100 kN load cell. The gauge length/specimen width was 150/16 mm and 170/16 mm for the 34–700 and T700SC specimens, respectively. The length/width/thickness of the woven E-glass/epoxy composite end tabs were 50/15/4 and 40/16/4 mm, respectively. The displacement rate was 0.5 and 1 mm/min for the seven 34–700 and ten T700SC specimens, respectively. An optical extensometer was used to measure the surface strain of the 34–700 specimens. The optical extensometer measured the relative displacement between two markers. Two-dimensional digital image correlation was used to measure the average longitudinal surface strain for the T700SC specimens.

Due to the use of the glass fibre layers, (1) the failure of the 34–700 or T700SC plies did not correspond to final failure of the specimen and (2) the determination of the stress in the 34–700 or T700SC plies required a back-calculation [58,59]. The failure of these plies was identified by a distinct stress drop in the stress–strain diagram. The thermal residual stresses were corrected for using Schapery's equations [62] and force equilibrium. This reduced the macroscale failure strain by just 0.044% and 0.040% for 34–700 and T700SC, respectively. The accuracy of the stress back-calculation was assured by (1) performing cross-sectional area measurements on every individual specimen of the glass/carbon hybrid specimens using optical microscopy and (2) measuring the tensile stiffness on UD glass fibre composites. The accompanying *Data in Brief* article [63] describes this back-calculation in more detail.

2.4. Microscale SRCT experiments

Double-notched specimens (see Fig. 1a) were cut by water jet from the cured panels, and 1 mm thick aluminium tabs were glued to the ends (see Fig. 1b) using 3 M Scotch-Weld EC 9323B/A. The adhesive was cured in a convection oven at 100 °C for 15 min for 34–700 specimens and at 60 °C for 1 h for T700SC specimens.

SRCT measurements were performed at the TOMCAT beamline at Swiss Light Source (SLS) by teams with members from KU Leuven, INSA Lyon and the University of Southampton. These measurements used the INSA Lyon tension–compression rig, which recorded both load and displacement [64]. The displacement rate was chosen to reach failure within 7–10 min. Some differences in strain rate may be inevitable, but they are unlikely to be significant. The GigaFRoST camera was used to enable continuous scanning [65]. Table 1 summarises further details of the experimental settings. Absorption-based reconstruction was performed using the in-house algorithms supplied by SLS. 16 to 19 scans were reconstructed and analysed per specimen. Fig. 2 shows example slices for both material types to illustrate the relatively uniform fibre distribution, low void content and overall specimen quality. Water jet cutting did introduce some through-thickness tapering (see Fig. 2a and c), but no visible damage. Splits (see Fig. 2d) occurred at 55–65% and 40–50% of the failure load for 34–700 and T700SC, respectively, and hence removed the stress concentration caused by the notch in the imaged region. No preferential fibre break development near the 90° plies nor along the specimen length, within the field of view, were observed.

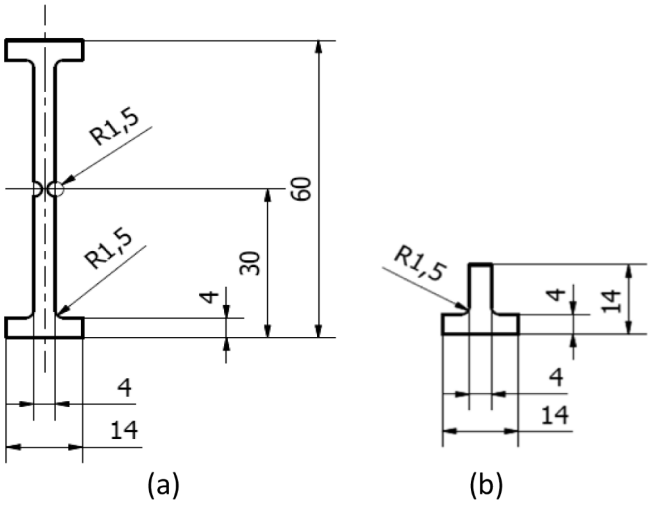

Fig. 1. Double-notched specimen design for SRCT measurements: (a) the specimen itself and (b) the aluminium end tab. All dimensions are in mm.

The SRCT scans were used to analyse the fibre alignment using VoxTex [66], and Table 2 summarises the results. The void content was found to be so low that it could not be accurately quantified.

2.5. Microscale SRCT data analysis

The data analysis started by rotating the SRCT volumes to the same specimen orientation, and cropping to the specific region of interest. The last volume before failure was analysed in detail for fibre breaks by several manual inspections. The preceding volumes were then analysed to identify the scan in which the fibre breaks first appeared. The coordinates of all breaks were recorded for every volume, and were then used to check whether they belonged to a cluster (see Fig. 3). Fibre breaks were considered to be part of the same cluster if they were within a centre-to-centre radial distance of two fibre diameters and an axial distance of fifteen fibre diameters. These criteria were derived from FE models [25] assuming hexagonal packing and elastic-perfectly plastic matrix behaviour, using the tensile modulus and shear onset defined in section 3.2. Clusters containing 'n' fibre breaks are referred to as 'n-plets' [67].

For stress calculation purposes, the cross-sectional area of the 0° ply needed to be defined. In the last volume imaged before failure, ImageJ Fiji's [68] polygon tool was used to mark the contour of the 0° plies, and measure the area in px^2. This value was converted into area in mm^2 by using the voxel size in Table 1. It should be noted that the last volume may have a slightly smaller cross-sectional area than the first volume due to Poisson's contraction. However, the effective 0° ply area cannot be accurately determined in the first volume, because the splits along the notch have not occurred yet. The longitudinal stress was calculated as the load divided by the 0° ply area, hence ignoring the contribution of the 90° plies. This is reasonable as the 90° ply contributions to the load carrying capacity is limited, even in the absence of transverse cracks and delaminations. During the tests, transverse cracks first appeared in volumes at 9–51% of the failure load, depending on the specimen. Local delaminations were seen in some cases, but their crack openings were too small to make their detection straightforward. The presence of the 90° plies/cracks was not reflected in increased fibre break densities near the 0/90 ply interface, as exemplified in Fig. 3.

Table 1
SRCT test and scan parameters for the *in-situ* microscale tensile tests.

	34–700	T700SC
Sensor size (px^2)	2016 × 2016	
Pixel size (μm)	11.0	
Energy (kV)	20	
Exposure time (ms)	9	
Microscope magnification	10×	13.7×
Voxel size (μm)	1.1	0.8
Number of projections/volume	1000	1500
Propagation distance (mm)	60	170
Displacement rate (μm/s)	1.4–1.6	2.3–2.4
Number of volumes acquired before failure	60–62	33–37
Total testing time (min)	9–9.3	7.4–8.3

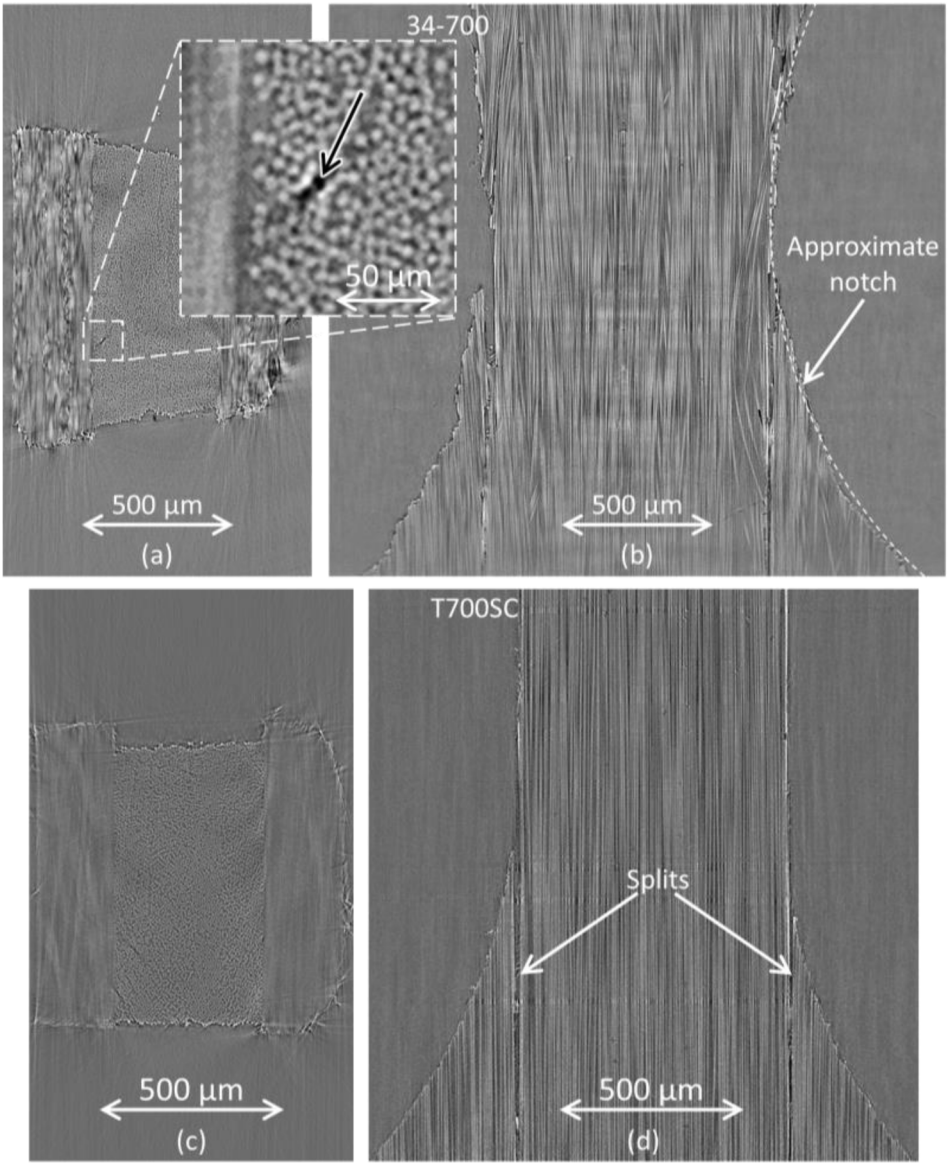

Fig. 2. Example of SRCT data showing the specimen quality: (a) cross-sectional slice of a 34–700 specimen, (b) longitudinal slice of a 34–700 specimen, (c) cross-sectional slice of a T700SC specimen and (d) longitudinal slice of a T700SC specimen. All these slices were taken from the last volume before failure. The arrow in the inset in (a) reveals the presence of a single fibre break.

Table 2
Analysis of the fibre orientation of the 4 microscale specimens.

Material	Specimen #	In-plane orientation	Out-of-plane orientation
34–700	1	0.6° ± 3.0°	0.0° ± 1.6°
	2	0.4° ± 3.5°	−0.3° ± 1.3°
T700SC	1	−0.5° ± 4.9°	−1.0° ± 5.4°
	2	−3.5° ± 6.6°	0.2° ± 6.0°

The fibre volume fraction V_f was measured by first counting individual fibres in a given CT cross-section using the Insegt Fibre algorithm developed by Emerson et al. [69]. After manual confirmation of the accuracy of the algorithm, this information was combined with the fibre diameter measurements (see section 3.2) to calculate the V_f. The standard deviation was obtained by performing this analysis on about 30 CT cross-sections. The results are described in section 3.2.

3. Model description

3.1. Models

Six different models will be compared with each other as well as with experimental results. These models have been described in detail in the literature (see Table 3). All six models are based on the same two key features: (1) using the Weibull distribution for fibre strength to predict at which stress level fibres will fail, and (2) applying stress redistribution around fibre breaks. All models have essentially used the same Weibull distribution with one small exception for ABS, which will be explained in section 3.2. The main differences therefore arise in how the models handle stress redistribution around fibre breaks. DFBM handles this in the simplest manner: the stress is redistributed over all remaining fibres, and a shear lag theory is applied for the stress recovery along the broken fibre. ABS and HSL also use shear lag theories for the stress recovery along the broken fibre, but they are different from DFBM in terms of how they distribute the load over the neighbouring fibres. ABS distributes the load over the six nearest neighbours in a hexagonal packing, whereas

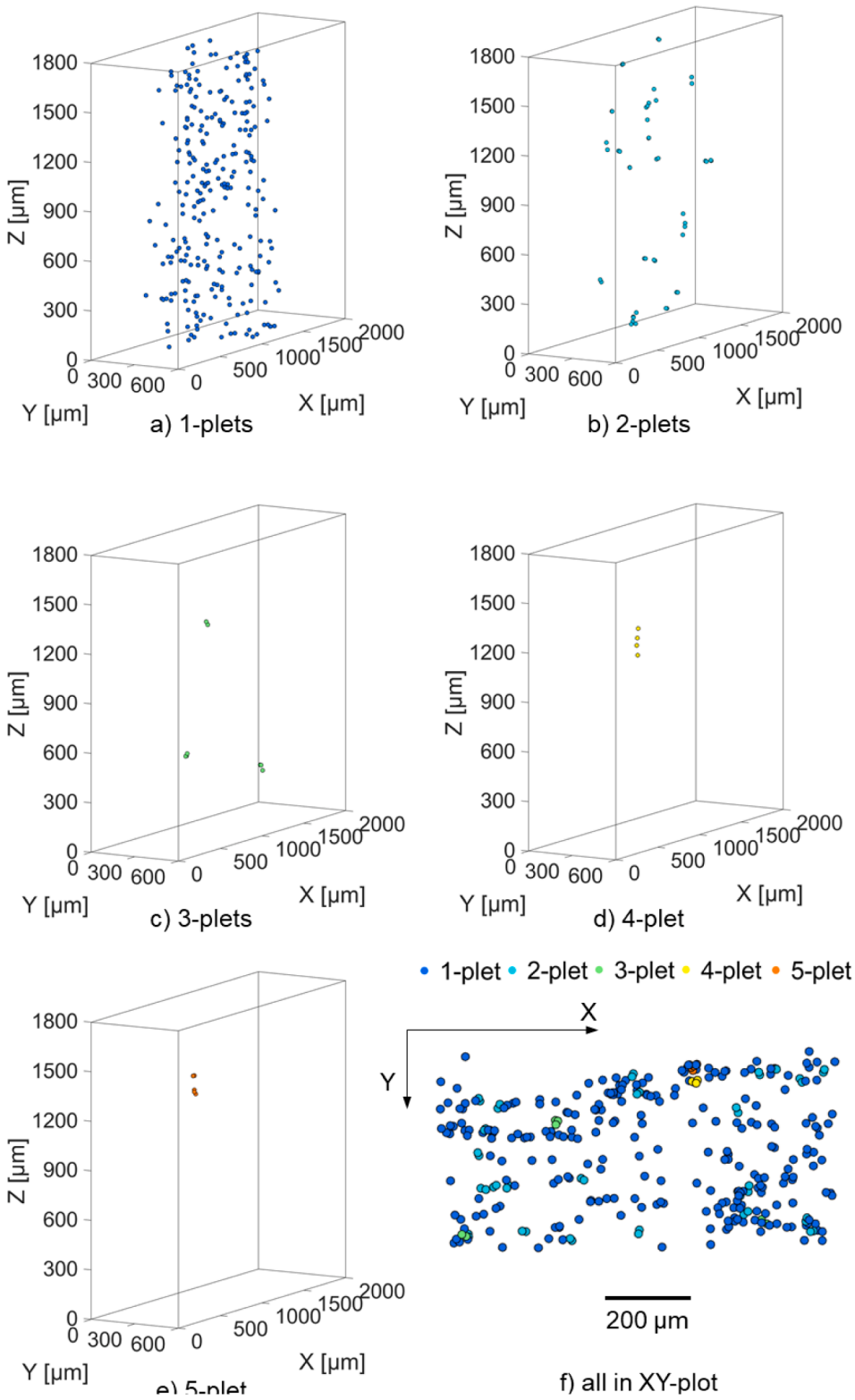

Fig. 3. Fibre breaks and clusters present in the final volume before failure for one of the 34–700 specimens: (a) 1-plets, (b) 2-plets, (c) 3-plets, (d) 4-plets and (e) 5-plets in a 3D view, and (f) all breaks and clusters projected onto the X-Y plane. The notch tip was located at the z = 1200 µm plane.

HSL sheds the load fully to the nearest neighbouring fibre (or cluster of fibres of the same size as the broken cluster). 3PFM, DYSEM and FEISM have more complex stress redistribution rules, which are either based on calibrated analytical functions (3PFM), equilibrium equation from a spring element model (DYSEM) or finite element models (FEISM). The models are also significantly different in their implementation and, therefore, in their computational cost: DFBM and HSL are probabilistic analytical models, thus requiring only one run to calculate the representative response of a composite material; the other models are based on Monte Carlo numerical simulations, thus requiring several runs to calculate representative responses. Table 4 presents a more detailed overview of the main features and assumptions of the six models.

Table 3
The six models, their acronyms, and some key references.

Full name	Acronym	Institution	References
3D progressive failure model	3PFM	University of Girona	[40,94]
Analytically based-strength simulation	ABS	National Physical Laboratory and Ghent University	[37,95]
Dispersed fibre breaks model	DFBM	University of Aveiro	[96]
Dynamic spring element model	DYSEM	University of Porto	[32,33,97]
Finite element-imposed stress model	FEISM	KU Leuven	[10,16,24,25,98–100]
Hierarchical scaling law	HSL	Imperial College London	[35,54]

Given that they constitute the most important difference between the models, the stress redistributions around fibre breaks will be compared in detail in section 4.1 before proceeding with the comparisons against experiments. Their predictions for two virtual materials have been compared in [70]. In this study, 3PFM and FEISM submitted the results of 50 Monte Carlo runs, whereas ABS and DYSEM submitted the results of 10 runs. DFBM and HSL are probabilistic models and hence submitted only the statistically expected values (and, for HSL, standard deviations).

3.2. Modelling parameters

Table 5 summarises the fibre-related properties. The diameter and the Weibull parameters were taken from single fibre tensile tests performed using the LEX/LDS automated testing equipment at Dia-Stron Limited, as described in Mesquita et al. [71]. The maximum likelihood estimator was used to obtain the Weibull scale parameter σ_0, Weibull modulus m and Weibull reference gauge length L_0, assuming a unimodal distribution. A total of 89 and 92 measurements were used to determine the Weibull parameters for the 34–700 and T700SC fibres, respectively (see Fig. 4). The choice of a unimodal Weibull distribution was motivated by (1) some models being unable to handle other types of distributions, (2) the absence of any experimental indications of multiple flaw types to justify using a bimodal Weibull distribution [4] and (3) a lack of enough data at other gauge length to establish a power-law accelerated or Weibull-of-Weibull distribution [5–9]. Nevertheless, all individual diameter and strength measurements were also provided to the participants, and they are publicly available on [72]. Interested readers can therefore fit other distributions to the data and analyse the effect on the predictions. The elastic and thermal constants in Table 5 are based on the literature [58,73–78], apart from the longitudinal modulus E_{11} being taken from the manufacturer's data sheet for the carbon fibres. DYSEM also used a carbon fibre and matrix density of 1800 kg/m^3 and 1200 kg/m^3, respectively, and a damping coefficient of 0.01.

The stress–strain diagrams of the neat resin were measured using the methodology described in Morelle et al. [79], which combines compressive and tensile testing of neat resin specimens using a Drucker-Prager yield criterion. The participants were provided with tension, compression and shear stress–strain behaviour (see Fig. 5). The tensile moduli were 3.15 GPa and 3.36 GPa for the 736LT and SR8500 resins, respectively. The shear onsets, which were defined as the maximum shear stress prior to softening, were 60.4 and 63.3 MPa for 736LT and SR8500, respectively. This definition of shear onset, which was suggested as the best shear yield stress estimate for models assuming perfect plasticity, was used by all models. The Poisson's ratios were measured to be 0.39 and 0.42 for 736LT and SR8500, respectively. The coefficient of thermal expansion for epoxy was estimated to be 62.5 10^{-6}/K [58,75,76].

Table 6 summarises the geometrical parameters of the two composite systems considered by the models. The actual data analysis was performed after the results were submitted by the modelling participants, and this led to some minor discrepancies with the micro- and macroscale specimens (see Table 6). The micro- and macroscale strength and stress values were, therefore, linearly normalised with respect to the V_f that was provided to the participants.

The modelling participants were recommended to use the distance-based criterion for defining clusters, as described in section 2.5. The benchmarking exercise was run blind: none of the participants had seen the outcome of the experiments nor each other's predictions by the time they submitted the requested results.

4. Results

4.1. Modelled stress redistribution

The modelling participants extracted axial stress redistribution for four simple cases: a single fibre fracture and two adjacent co-planar fibre fractures, each at an applied strain of 1% and 2%, while all other fibres are intact. These models were run for hexagonal packing using the constituent properties, geometry and V_f of the 34–700 case. Fig. 6 summarises these results for the six models. ABS only provided results for the single fibre fracture case. For DYSEM, only the static stress redistributions are shown to enable a fairer comparison. Its peak dynamic stress concentrations on the nearest neighbour intact fibres were between 17% and 48% higher for the cases reported here.

- HSL predicts a stress concentration of 100% in the intact fibres, which is much higher than any of the other models. This value, however, does not change with cluster size, and hence the difference relative to other models would become smaller with increasing cluster size.
- DYSEM and FEISM are the only two models that predict regions with negative stress concentration in the intact fibres. This is because FEISM is based on FE models and DYSEM on a simplified FE model (=spring element model). These negative values are commonly reported [22–27], and are attributed to the requirement of maintaining overall strain compatibility.
- FEISM is the only model that predicts the maximum stress concentrations in the intact fibres to occur away from the fibre break plane. This observation is in line with other FE models [22,26].
- For computational efficiency reasons, FEISM always uses the stress redistributions at an applied strain of 2%, irrespective of the actual applied strain. Its FE model would predict different profiles at 1% strain, but they are not used in the strength model and hence are not shown.
- DFBM spreads the stress concentrations over all remaining intact fibres. These stress concentrations, therefore, are very low and the same for all intact fibres. They are not shown in Fig. 6b and d.
- ABS predicts stress concentrations in the six nearest neighbours that are uniform over the entire element length (500 μm), whereas those in the other models decrease over a significantly shorter length.
- After DFBM, 3PFM has the lowest stress concentrations in the intact fibres, and the maximum value does not change with increasing applied strain. DYSEM does predict a smaller stress concentration at larger applied strains due to the increased yielding of the matrix.
- Both DYSEM and DFBM assume linear elastic-perfect plastic matrix behaviour, and thus predict the same stress recovery around a single broken fibre (see Fig. 6a). In contrast with DYSEM, DFBM does not capture the effect of multiple fibre breaks on the stress recovery, and therefore, predicts steeper stress recovery for the case of two broken fibres (see Fig. 6c).

4.2. Basic results

Fig. 7 displays the failure strains predicted for both cases and

Table 4
Overview of the key features of the six participating models (reprinted from Breite et al. [70], with permission from Elsevier).

Feature		3PFM	ABS	DFBM	DYSEM	FEISM	HSL
Material response	Elastic properties of fibre	Linear elastic up to failure, isotropic. Non-linear elastic behaviour can be incorporated in an approximate manner.	Linear elastic, transversely isotropic.	Linear-elastic, no consideration of anisotropy.	Linear elastic, isotropic. Non-linear elastic behaviour can be incorporated in an approximate manner.	Linear elastic, transversely isotropic. Non-linear elastic behaviour can be incorporated in an approximate manner.	Linear-elastic, no consideration of anisotropy.
	Fibre strength distribution	Standard implementations for unimodal, bimodal and PLAW available, but others can easily be plugged in.	At the moment, unimodal distribution only, but others can easily be plugged in. Strength values smaller than half of the mean or larger than two standard deviations above it are rejected.	At the moment, unimodal distribution only. Equations need to be reworked for other Weibull distributions.	Standard implementations for unimodal, bimodal, WOW and PLAW available, but others can easily be plugged in.	Standard implementations for unimodal, bimodal and PLAW are available, but others can easily be plugged in.	At the moment, unimodal distribution only. Equations need to be reworked for other Weibull distributions.
	Matrix	Perfectly plastic (elastic also possible)	Linear elastic (perfectly plastic in shear if debonding would be present)	Linear elastic-perfectly plastic	Linear elastic-perfectly plastic. More complex behaviours can be used.	Linear elastic-(nearly) perfectly plastic. More complex behaviours can be used.	Perfectly plastic in shear, considered in combination with the interface.
	Interface	Perfect bonding assumed. In principle possible to add this effect approximately.	Perfect bonding assumed here, but can be taken into account.	Perfectly plastic in shear, considered in combination with the matrix.	Perfect bonding assumed. Prepared for taking debonding into account but not done yet.	Perfect bonding assumed. In principle possible to add this effect approximately.	Perfectly plastic in shear, considered in combination with the matrix.
Fibre packing type	Random (regular also possible)	Hexagonal	Hexagonal	Random (regular also possible)	Random (regular also possible)	Square (hexagonal also possible)	
Stress concentrations	Near individual fibre breaks	Analytical function calibrated with FE simulations and a spring element model.	Analytical model based on equilibrium equations, interface continuities and stress–strain equations, load shared by six nearest neighbours	Shear lag along the fibres, load shared by all remaining fibres	Actual stress redistribution from equilibrium equations, including dynamic stress concentrations.	3D FE model to capture the entire stress redistribution. Modelled at 2% macroscopic strain.	Shear lag, considering that all excess load is carried by one neighbouring fibre.
	Near multiple fibre breaks	Linear superposition; the model captures the increase in ineffective length with cluster size, but only if the breaks are located at the same plane.	Load shared by all nearest neighbours to the cluster.	Not relevant	Superposition not necessary. The model captures the increase in ineffective length with cluster size.	Enhanced superposition principle, which is accurate in plane. The increase in ineffective length is not captured, but addressed in ongoing work.	Shear-lag, considering that all excess load is carried by one neighbouring cluster of the same size as the broken cluster.
Clusters of fibre breaks	Definition	Distance-based criterion. Can be changed according to the specifications	Distance-based criterion. Can be changed according to the specifications	Cannot be tracked.	Distance-based criterion. Can be changed according to the specifications	Distance-based criterion. Alternative criterion based on the % of SCF also available.	A cluster is defined by fibre breaks/sub-broken-clusters with interacting recovery regions.
	Cluster sizes	Any size is possible	Any size is possible	Not applicable	Any size is possible	Any size is possible	1, 2–3, 4–7, …
	Coplanarity	Can monitor coplanarity, but does not enforce it.	One cell covers more than one ineffective length, which prevents stress concentrations from affecting cells in other layers.	Does not consider clusters of fibre breaks, but the co-planar breaks condition can be enforced	Can monitor coplanarity, but does not enforce it.	Can monitor coplanarity, but does not enforce it.	Does not impose co-planar breaks to calculate failure probabilities, but does assume co-planar breaks to model stress fields near broken clusters

(*continued on next page*)

Table 4 (*continued*)

Feature	3PFM	ABS	DFBM	DYSEM	FEISM	HSL
Matrix contribution to composite stress calculation	Linear elastic matrix contribution included	Linear elastic matrix contribution included	Not included	Not included	Linear elastic-perfectly plastic matrix contribution included	Not included
Simulation type	Monte Carlo	Monte Carlo	Probabilistic	Monte Carlo	Monte Carlo	Probabilistic
Information regarding pre-calculations	Generation of the random packing is run prior the start of the simulation.	No pre-calculations needed	No pre-calculations needed	Generation of the random packing is run prior the start of the simulation.	FE simulations are needed for a non-standard carbon fibre or new matrix behaviour. Basic library of fibre–matrix combinations is available. Generation of the random packing is run prior the start of the simulation.	No pre-calculations needed
Determination of final failure	When either a load drop of 10% is detected or all fibres in a cross-section are broken.	When just one axial layer of elements has failed completely after the system becomes unstable due to an avalanche of fibre breaks. Other criteria are available.	By the maximum stress that the representative volume element can withstand	When the stress drops below 90% of the maximum stress.	When an avalanche of fibre breaks occurs without any increase in macroscopic strain. The model captures this through a rising number of fibre breaks per iteration for the same strain increment.	When the bundle cannot carry any additional load.

compares them with macroscale experimental measurements. The measured failure strain of 34–700 (1.65% ± 0.11%) is below the data sheet value (2.0%), whereas it is relatively close for T700SC (1.96% ± 0.05% versus 2.1%). 3PFM, DFBM, DYSEM and FEISM overpredict significantly the measured failure strain for both cases, whereas ABS and HSL are reasonably close.

Fig. 8 plots the tensile strength predictions for both cases against the strength measured in macro- and microscale experiments. Model predictions show similar trends as for failure strain:

- 3PFM, DFBM, DYSEM and FEISM overpredict strength.
- ABS and HSL's predictions are both close to the macroscale strength measurements, with ABS's being slightly higher than HSL's (although the relationship between (i) the precise value of model predictions and (ii) the experimental results should not be interpreted as a measure of model accuracy, as will be discussed later in this section and in Section 5).

The differences between the micro- and macroscale strength values are not statistically significant with p-values of 0.34 and 0.054 for 34–700 and T700SC, respectively. Note that most previous research has tested only one specimen and did not compare data with macroscale specimens [16,42–47]. This will be elaborated in section 5.

Fig. 9 depicts the stress–strain diagrams for both composites. In addition to the earlier observations related to failure strain and strength, Fig. 9 reveals that, apart from HSL, all models predict significant non-linearity. This will be elaborated in section 5.

Fig. 10 displays the fibre break density for the 34–700 and T700SC cases, which is defined as the number of fibre breaks in the analysed volume divided by the volume. The Weibull predictions are based on the expected number of fibre breaks for the volume or length of fibres present in the absence of any stress redistributions around fibre breaks. The following observations are made:

- The results of the two microscale specimens are very consistent for both cases (see Fig. 10). This is even the case for the fibre break densities at failure.
- 3PFM, DYSEM, FEISM, HSL and the simple application of Weibull statistics overpredict the fibre break density evolutions for both cases, which strongly suggests that the Weibull distribution used as input for these models was not representative of the real strength distribution of the fibres inside the tested specimens. Nevertheless, a large number (89–92) of single fibre tensile tests were performed to characterise the fibre strength distribution, and the Weibull fit of the T700SC single fibre test data was reasonably good (see Fig. 4), especially when compared to the literature [4,6,15,80]. Since the model predictions are quite sensitive to fibre strength distribution inputs, good agreement with experimental results must be interpreted cautiously, as it is not a meaningful indication of model accuracy. This will be further discussed in Section 5.
- The initial predictions match well the Weibull predictions for all models, apart from ABS. At higher stress levels, the models start predicting higher densities than the Weibull predictions due to the presence of stress concentrations.
- The fibre break densities at failure are far too high compared to the experimental values for 3PFM, DYSEM and FEISM. Such high densities imply that many fibres contain multiple breaks in the imaged region. Multiple fibre breaks within a fibre have been experimentally observed, albeit at a lower frequency [57].
- ABS assumes that fibre strength values smaller than half of the mean fibre strength (at a gauge length of 500 μm) do not occur in practice. This threshold in ABS corresponds to around 1850/2380 MPa composite stress or 3690/4130 MPa fibre strength for 34–700/T700SC. The experimental data in Fig. 4 and Fig. 10 reveal that fibre breaks formed at much lower stresses are actually found in practice. We can therefore reject this ABS model assumption, which explains why its

Table 5
Properties of the fibre types: diameter, elastic constants [58,73–78], Weibull parameters and coefficients of thermal expansion (CTE) [75,76].

Fibre type	Diameter (μm)	E_{11} (GPa)	$E_{22} = E_{33}$ (GPa)	$G_{12} = G_{13}$ (GPa)	G_{23} (GPa)	$\nu_{12} = \nu_{13} = \nu_{23}$ (-)	σ_0(MPa)	m(-)	L_0(mm)	$CTE_L(10^{-6}/K)$	$CTE_T(10^{-6}/K)$
34–700	6.5	234	15	13.7	6	0.25	4306	5.1	12	−0.56	5.6
T700SC	6.8	230	15	13.7	6	0.25	4219	4.14	12	−0.56	5.6
HYBON 2026	–	82.7	–	–	–	–	–	–	–	5.4	5.4
SCG75	–	86.9	–	–	–	–	–	–	–	1.6	1.6

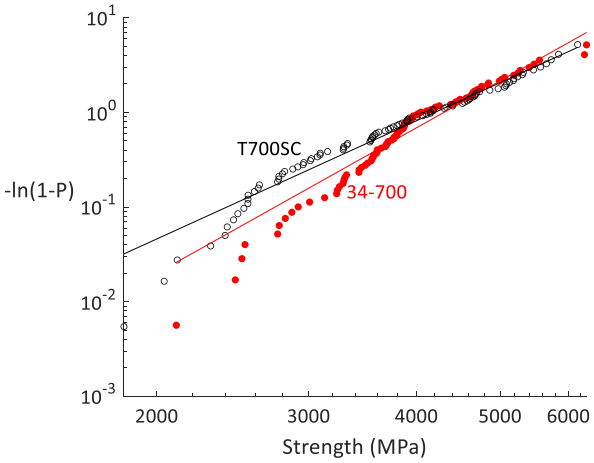

Fig. 4. Weibull plot for 34–700 and T700SC single fibre tensile test results. P represents the cumulative failure probability at the corresponding stress level, and ln is the natural logarithm.

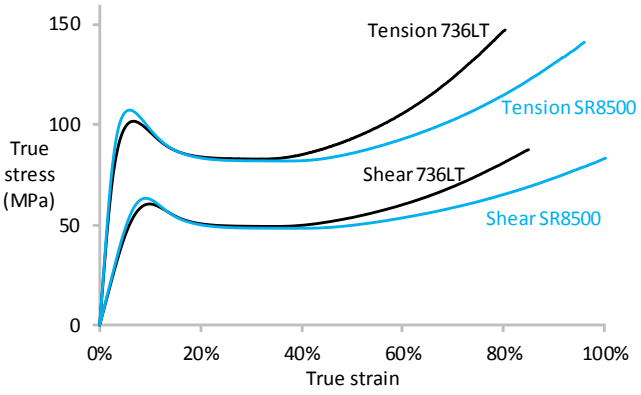

Fig. 5. True stress–strain behaviour of both resin types in shear and tension.

Table 6
Geometrical parameters recommended to the modelling participants. The actual values for the micro- and macroscale specimens are also included. Microscale specimens #1 and #2 will subsequently be indicated by '+' and 'o'-markers in the plots, respectively.

Composite		0° V_f (%)	0° width (mm)	0° thickness (mm)	0° area (mm^2)	Length (mm)	0° volume (mm^3)	Number of 0° fibres
34–700	Modelled	48.3 ± 0.4	0.91	0.44	0.40	1.20	0.48	5850
	Microscale #1	48.3 ± 0.4	–	–	0.44	1.76	0.76	6335
	Microscale #2	49.7 ± 0.5	–	–	0.44	1.73	0.76	6608
	Macroscale	52.5 ± 3.2	–	–	–	–	–	–
T700SC	Modelled	57.9 ± 0.7	0.74	0.38	0.28	1.20	0.33	4430
	Microscale #1	57.9 ± 0.7	–	–	0.31	1.14	0.35	4939
	Microscale #2	63.7 ± 2.4	–	–	0.25	1.20	0.30	4338
	Macroscale	52.1 ± 2.6	–	–	–	–	–	–

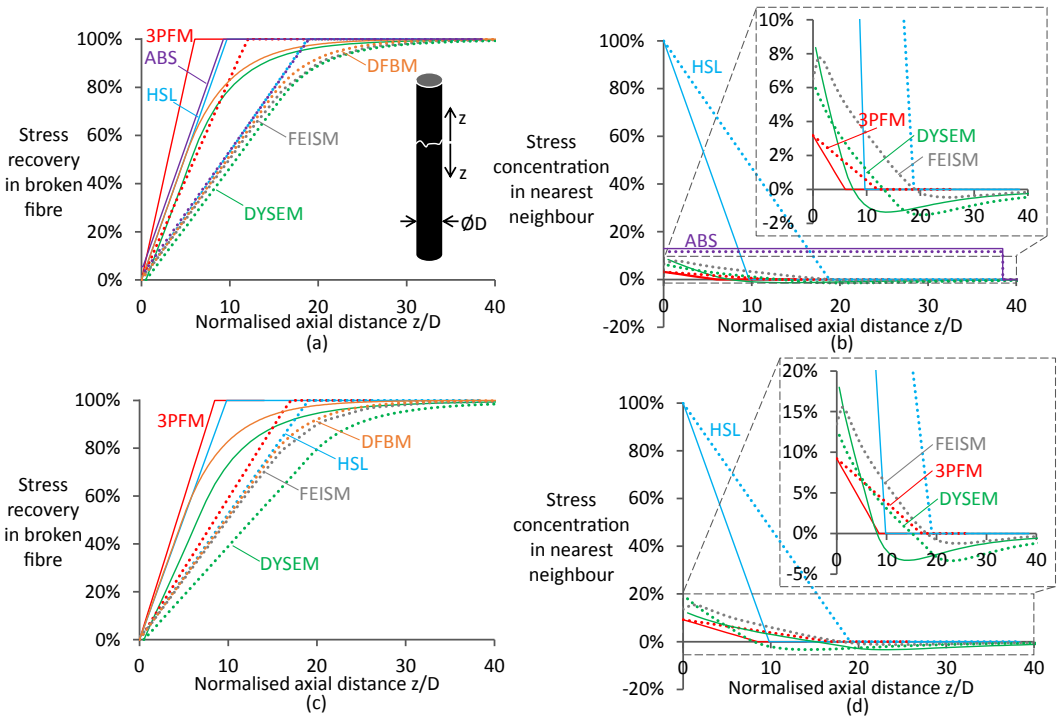

Fig. 6. Stress redistributions for hexagonal packings using the 34–700 data: (a) stress recovery for a single broken fibre, (b) stress concentration in the nearest neighbour for a single broken fibre, (c) stress recovery for two broken fibres, and (d) stress concentration in the nearest neighbour for a two broken fibres. The axial distance z from the fibre break is normalised by the fibre diameter D. Solid lines are for an applied strain of 1%, whereas dashed lines are for an applied strain of 2%. The DYSEM stress redistributions do not include the dynamic contribution, which was 17–48% higher than the static values.

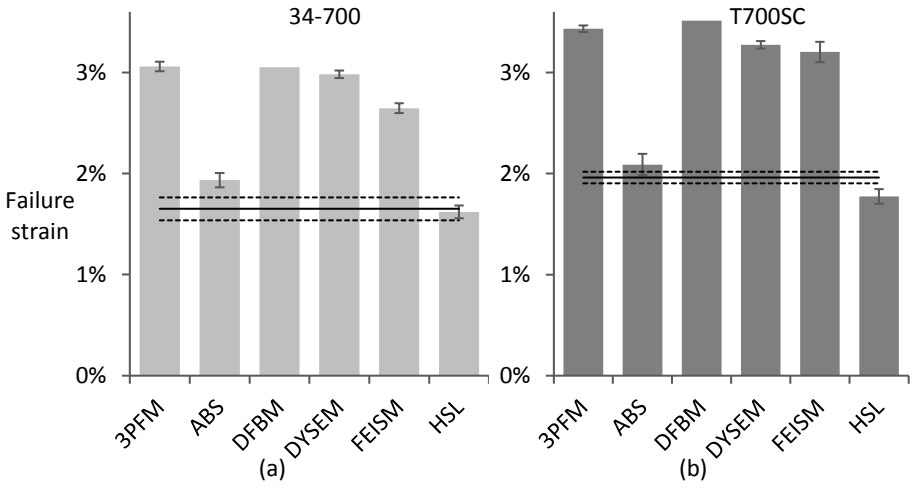

Fig. 7. Predicted and measured failure strains: (a) for 34–700 composites and (b) for T700SC composites. The bars represent the average of the Monte Carlo simulations or the expected values for the probabilistic models (DFBM and HSL), with error bars representing the standard deviation. The solid black lines represent the average of the failure strains measured in the macroscale experiments, with the dashed lines representing their standard deviations.

fibre break development starts much later than in the other models and in the microscale experiments. Based on the data presented here, we cannot make an objective assessment of the validity of discarding of strength values larger than two standard deviations above the mean, as also done by ABS.

4.3. Cluster development

This section describes the development of clusters of fibre breaks, as defined by the radial and axial distance criteria introduced in section 2.5. Fig. 11 shows the development of average largest cluster size as a function of applied stress. The evolution is captured reasonably well by all models, especially for the 34–700 case. The cluster sizes at failure are, however, overpredicted by most models, although HSL and ABS are very close for the 34–700 case. These good predictions should, however, be interpreted in the context of the overpredicted fibre break density in Fig. 10. Therefore, the better average largest cluster size predictions of HSL and ABS models are not a meaningful demonstration of improved accuracy; this will be further discussed in Section 5.

Fig. 12 reveals the density developments of 2-plets and 3-plets, which are clusters of 2 and 3 fibre breaks, respectively. Since HSL inherently groups 2-plets and 3-plets together, Fig. 12e and f also show

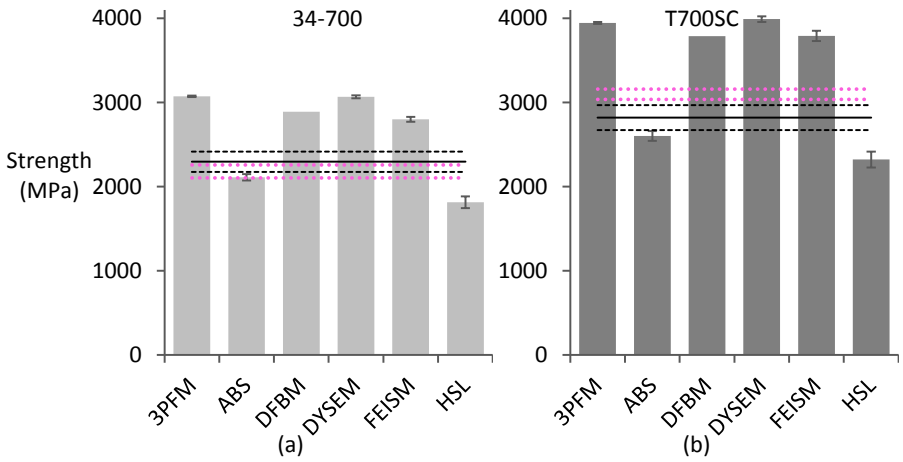

Fig. 8. Predicted and measured strength values: (a) for 34–700 composites and (b) for T700SC composites. The bars represent the average of the Monte Carlo simulations or the expected values for the probabilistic models (DFBM and HSL), with error bars representing the standard deviation. The solid black lines represent the average of the strengths measured in the macroscale experiments, with the dashed lines representing their standard deviations. The dotted pink lines represent the strength values measured in the microscale SRCT specimens.

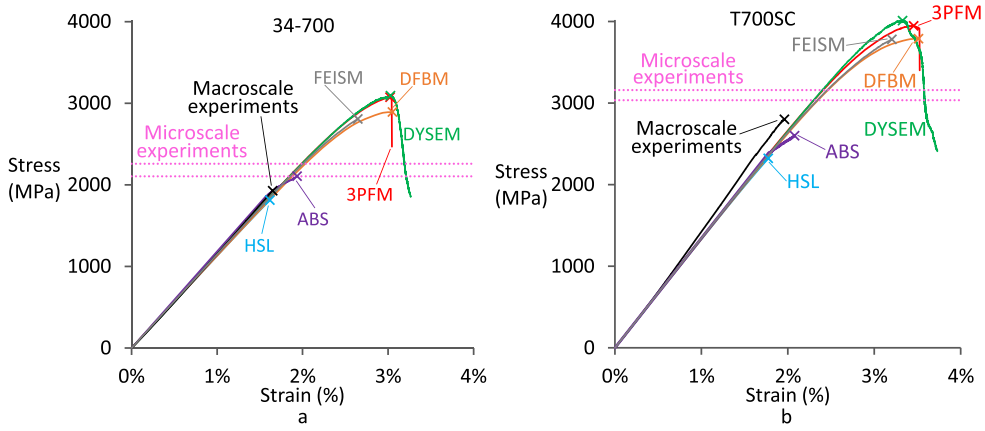

Fig. 9. Representative stress–strain diagrams for the (a) 34–700 and (b) T700SC predictions including the macroscale experimental results. The microscale strength values are represented by the pink dashed lines. The "×"-markers correspond to the failure point in the models.

the sum of the 2-plet and 3-plet density. In general, model predictions in Fig. 12 are better for the 34–700 case than for the T700SC case. Nonetheless, as mentioned above this must be interpreted in the context of the mismatch between fibre break density predictions and experimental values. HSL and ABS predict much lower 2-plet and 3-plet densities at failure than 3PFM, DYSEM and FEISM.

Fig. 13 depicts the cluster height standard deviation for 3-plets. This parameter is defined as the average standard deviation of the axial distance of every fibre break from its cluster centre, and is a measure for the coplanarity of the cluster. Due to the cluster definition (see section 2.5), the maximum value this parameter can reach, is 15 times the fibre diameter or 0.102 mm and 0.098 mm for 34–700 and T700SC, respectively. The three models that can monitor this parameter (3PFM, DYSEM and FEISM) overpredict it by a factor of 1.5 to 3. This indicates that clusters are significantly more coplanar in the experiments, as suggested earlier in the literature based on observations from a single specimen [16].

5. Discussion

The literature review showed that most other SRCT studies on fibre break development [16,42–47] did not test more than one nominally identical specimen, the exceptions being:

- Garcea et al. [48] reported many more isolated than clustered breaks in one specimen relative to the other.
- Schöberl et al. [49] found similar fibre break development for two nominally identical specimens, but one did not reach final failure. There were only 4 and 6 volumes available at different load steps.
- Rosini et al. [50] showed significant fibre orientation differences between two nominally identical specimens.

Besides involving two different materials, the present study is hence the first to analyse fibre break development up to failure of two nominally identical specimens, thereby providing a unique opportunity to assess specimen-to-specimen variation. The current results reveal a reasonable consistency between both specimens in terms of fibre break density (see Fig. 10) and 3-plet height standard deviation (see Fig. 13), but larger specimen-to-specimen variation for 2-plet and 3-plet density development (see Fig. 12) and largest cluster evolution (see Fig. 11). This was to be expected because fibre break density is based on several hundred observed breaks per specimen, whereas 2-plet, 3-plet and largest cluster measurements are based on one to two orders of magnitude fewer breaks. These cluster-related parameters may also have larger intrinsic scatter because they are likely to be governed by different mechanisms.

Table 7 analyses the variability in the strength, fibre break density and cluster development. Overall, model predictions display a similar level of variability as the microscale experiments for most of the parameters considered. This is encouraging, as it emphasises the repeatability of the experiments. For strength, this may have been a coincidence, as two specimens of 0.3–0.76 mm^3 are very likely to be

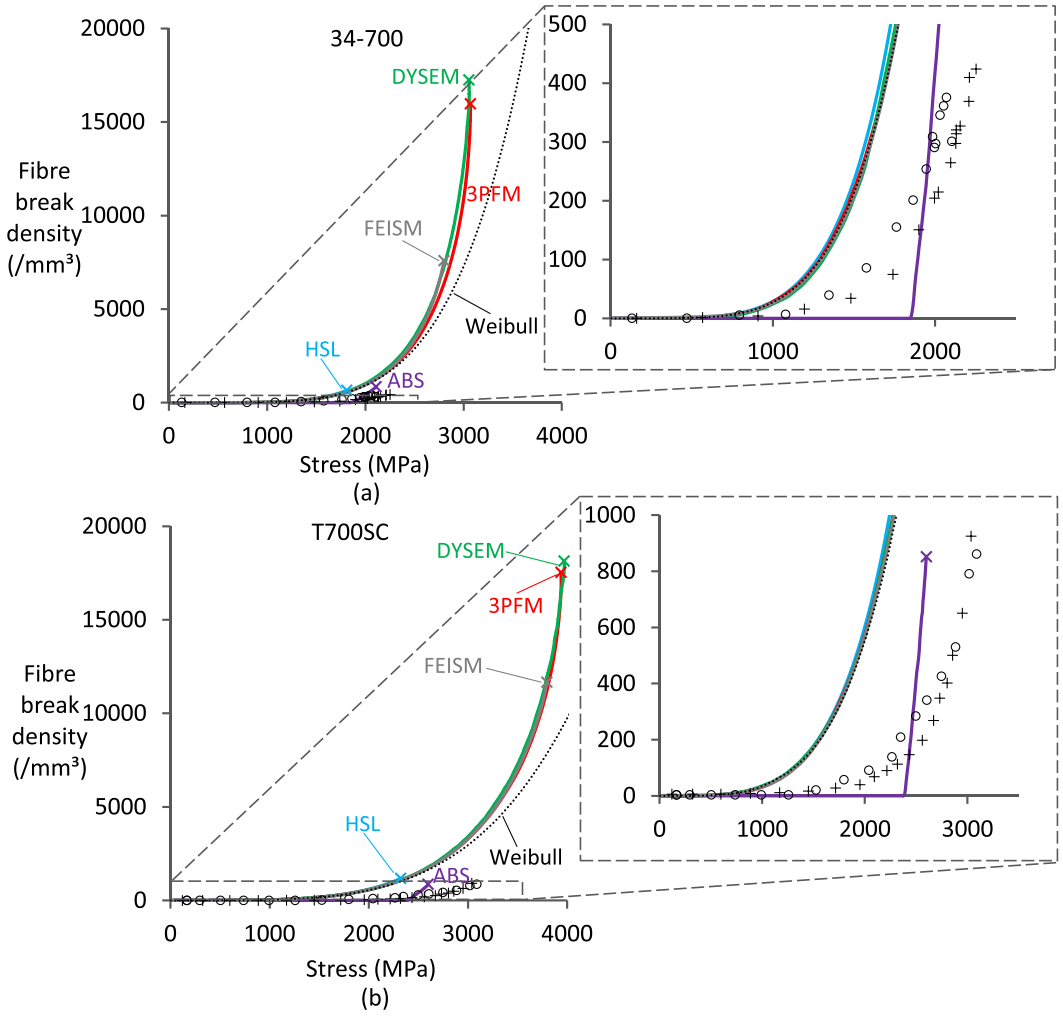

Fig. 10. Development of the fibre break density as a function of applied stress for the (a) 34–700 and (b) T700SC case. The "×"-markers correspond to the failure point in the models. The "+" and "o" markers correspond to the two experimental measurements per case. The model predictions were averaged over all simulations; for HSL, these data correspond to the statistically expected values (i.e. mathematical expectations).

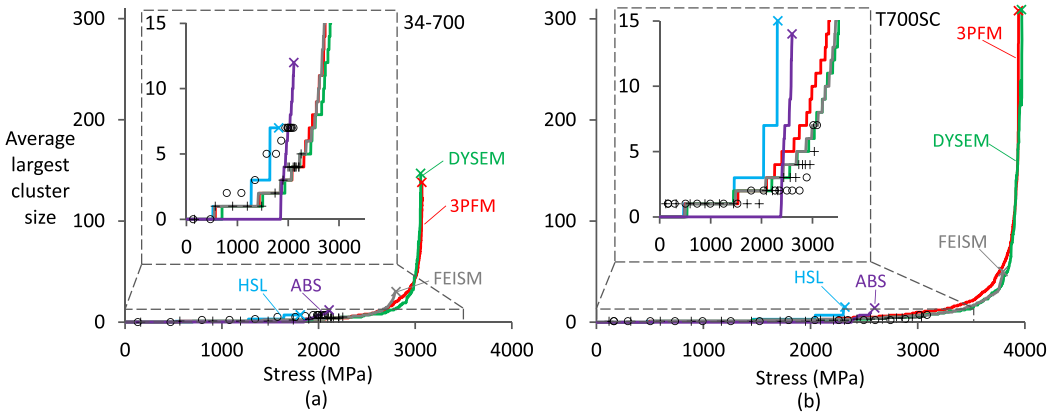

Fig. 11. Development of the average largest cluster size as a function of applied stress for the (a) 34–700 and (b) T700SC case. The "×"-markers correspond to the failure point in the models. The "+" and "o" markers correspond to the two experimental measurements per case. Model predictions were averaged over all simulations; for HSL, these data correspond to the expected values.

insufficient to measure strength reliably. For the fibre break density and cluster development, however, the present data are based on hundreds of fibre breaks and tens of clusters per SRCT specimen. The variability of the experiments is also much lower than the differences between the predictions from the various models. This shows that the experiments can be used to assess and distinguish the accuracy of the models.

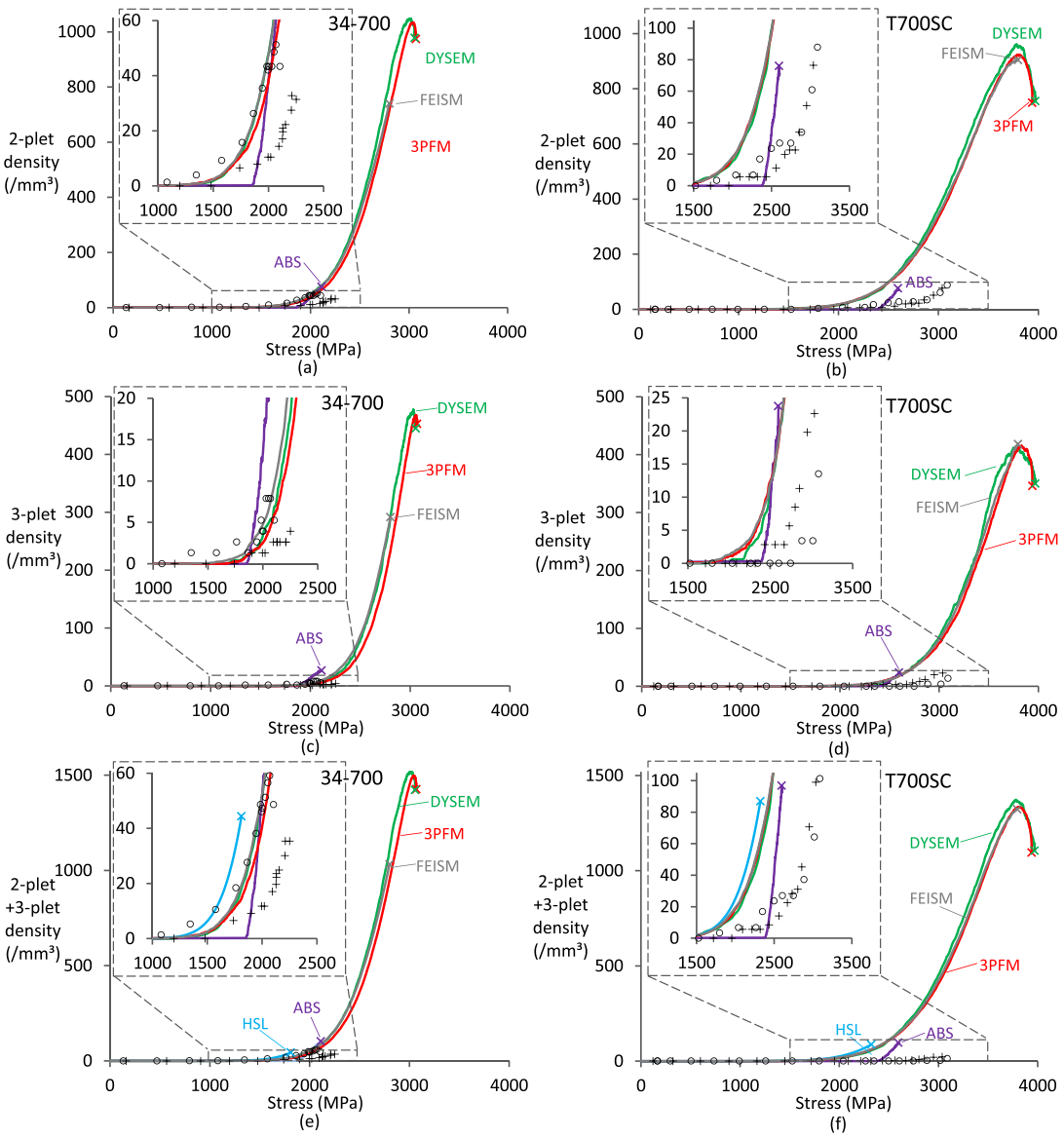

Fig. 12. Cluster density development as a function of applied stress: (a) 2-plet density for the 34–700 case, (b) 2-plet density for the T700SC case, (c) 3-plet density for the 34–700 case, (d) 3-plet density for the T700SC case, (e) 2-plet + 3-plet density for the 34–700 case and (f) 2-plet + 3-plet density for the T700SC case. The "×"-markers correspond to the failure point in the models. The "+" and "o" markers correspond to the two experimental measurements per case. Model predictions were averaged over all simulations; for HSL, these data correspond to the expected values.

All models, apart from HSL, predict significant softening in the stress–strain diagrams, which is not present in the macroscale results (see Fig. 9). For 3PFM, DFBM, DYSEM and FEISM, this softening, however, only occurs at much higher strains than the experimentally measured failure strain (see Fig. 10). This corresponds to the fact that most models overpredict the failure strain, which leads to excessive predicted fibre break densities and hence softening. The degree of softening predicted by the models is actually very low when analysed at the largest fibre break densities observed in the experiments, which ranged from 376 to 925 breaks/mm^3 (see insets in Fig. 10). The real issue therefore is that the models (apart from HSL and ABS) do not capture the failure point well, which leads to an overprediction of the fibre break density at failure. Note that the macroscale specimens even showed a stiffening of about 10% per 1% of applied strain for both cases (see Fig. 9). This is in line with experimental measurements of carbon fibre stiffening [81–84], which was not considered by any of the models, although 3PFM, DYSEM and FEISM have the facility to do so.

As described in section 4.2, the differences between the measured micro- and macroscale strength were not statistically significant. This shows that the features that may have affected this comparison were either negligible or cancelled out each other. The following factors were considered as being relevant:

- Size scaling may play a role, as the material volume under stress differs by almost three orders of magnitude between the micro- and macroscale specimens. Based on experimental size scaling data in the literature [6,85], this may lead to a strength increase of 10–20% relative to the macroscale strength.
- Damage introduced by water jetting or alignment issues may have reduced the microscale strength.
- The radiation exposure may have affected the mechanical properties of the polymer, making it more brittle and potentially lowering the composite failure strain. Although the fast scanning limited the total exposure (see Table 1), this effect cannot be fully excluded.
- A delayed failure of the carbon plies due to presence of the glass plies may have an influence on the macroscale strength. However, in the

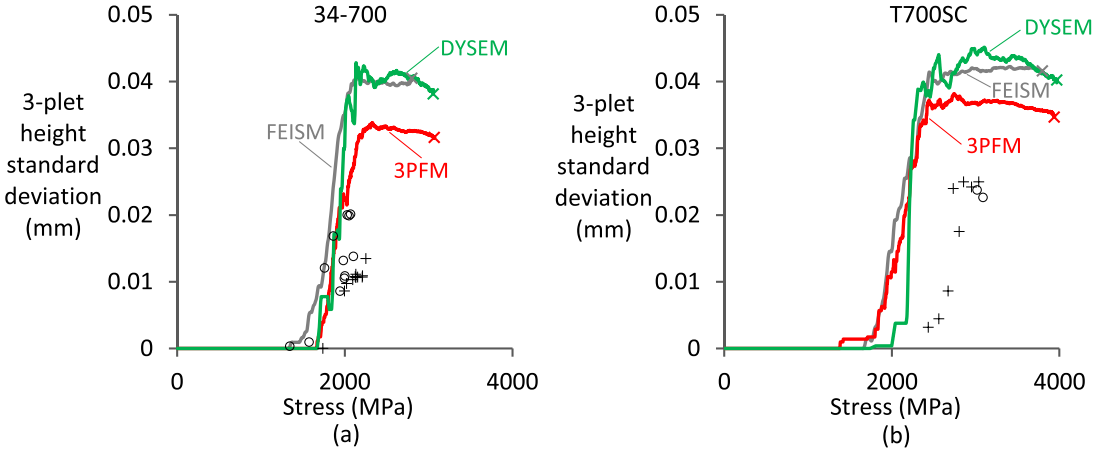

Fig. 13. 3-plet height standard deviation as a function of applied stress for the (a) 34–700 and (b) T700SC case. The "×"-markers correspond to the failure point in the models. The "+" and "o" markers correspond to the two experimental measurements per case. Model predictions were averaged over all simulations.

Table 7
Analysis of the variability of model predictions and experimental results at failure. CoV stands for the coefficient of variation. NA stands for 'not available'.

		Strength (MPa)		Fibre breakdensity (/mm^3)		Largest cluster size		2-plet density (/mm^3)		3-plet density (/mm^3)		2+3-plet density (/mm^3)	
		Average	CoV	Average	CoV	Average	CoV	Average	CoV	Average	CoV	Average	CoV
34–700	3PFM	3073	0.3%	17,287	4%	241	35%	1060	3%	488	6%	1548	3%
	ABS	2111	1.8%	353	21%	14	48%	31	18%	13	23%	44	18%
	DYSEM	3068	0.5%	17,812	6%	219	32%	1067	3%	495	5%	1561	2%
	FEISM	2799	1.0%	7686	10%	35	46%	733	8%	289	12%	1023	8%
	HSL	1814	3.9%	657	6%	4 to 7	NA	NA	NA	NA	NA	44	21%
	Experiments	2182	5.0%	400	9%	6	24%	41	34%	6	47%	47	36%
T700SC	3PFM	3945	0.3%	19,557	4%	1302	52%	954	5%	443	7%	1398	5%
	ABS	2603	2.3%	273	34%	12	59%	23	37%	8	51%	31	37%
	DYSEM	3991	0.8%	18,864	5%	381	48%	984	7%	436	8%	1420	6%
	FEISM	3792	1.6%	11,714	12%	56	70%	890	6%	406	9%	1296	5%
	HSL	2323	4.1%	1175	6%	8 to 15	NA	NA	NA	NA	NA	87	18%
	Experiments	3098	2.8%	894	5%	6	24%	82	10%	18	36%	100	2%

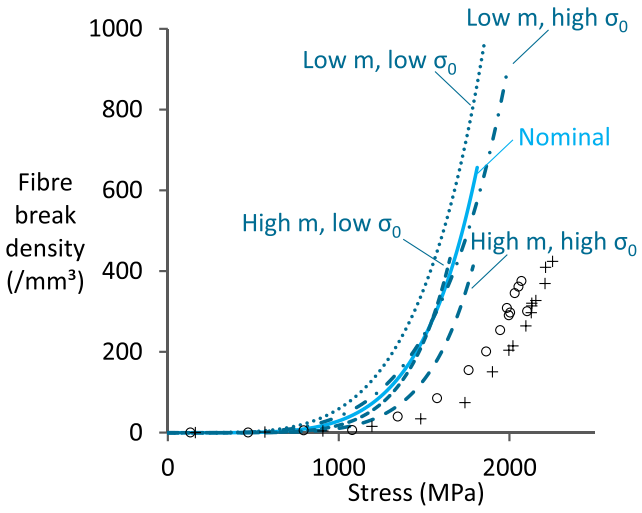

Fig. 14. Analysis of the uncertainty in the Weibull parameters on the HSL predictions for the 34–700 case.

present study this effect can be safely excluded: the blocked carbon ply thicknesses were three to five times larger than the thickness threshold identified by Wisnom et al. [59].

- The microscale experiments were performed on double-notched cross-ply specimens due to practical SRCT requirements. None of the participating models, however, included the strength decrease that the 90° plies and the notch may cause.
  - o An extended version of FEISM (and ABS [86]) can incorporate the effect of cracks in the 90° plies. Even though different input parameters were used, this model has shown that transverse cracks

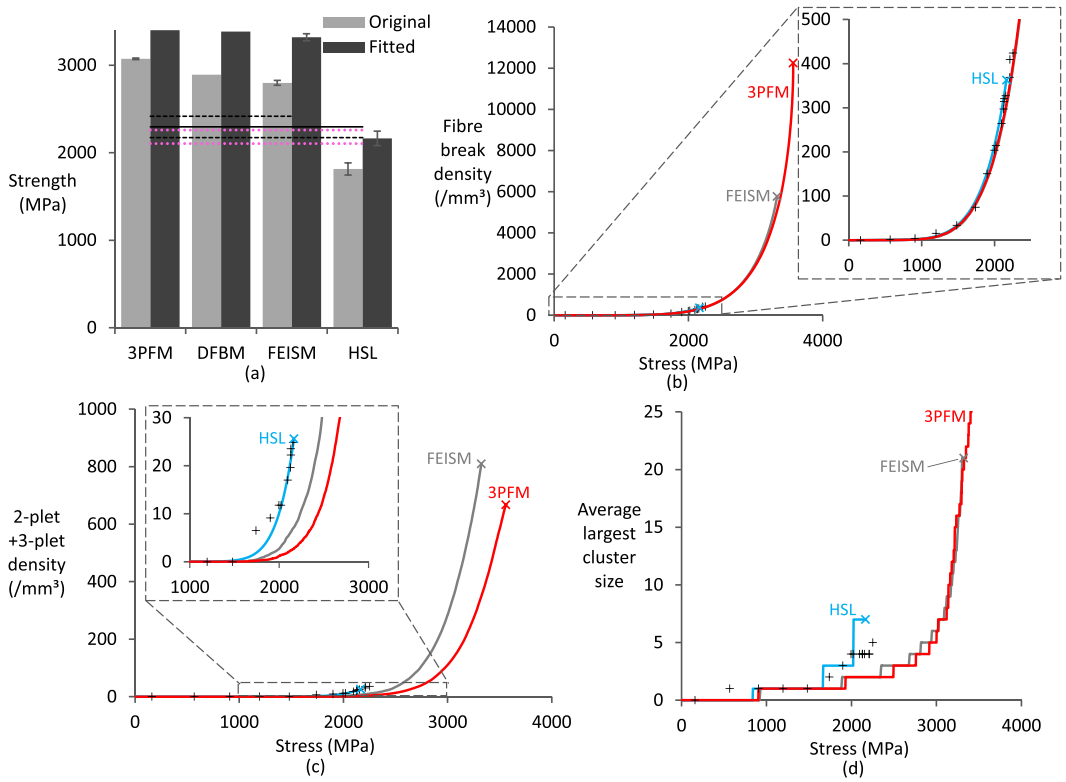

Fig. 15. Influence of a fitted Weibull strength distribution on predictions for the 34–700 case: (a) strength, (b) development of the fibre break density, (c) development of 3-plet density, and (d) largest cluster size as a function of applied stress. The solid black lines in (a) represent the average of the strengths measured in the macroscale experiments, with the dashed lines representing their standard deviations. The dotted pink lines in (a) represent the strength values measured in the microscale SRCT specimens. The "×"-markers correspond to the failure point in the models. The "+" markers correspond to the 34–700 SRCT specimen used to fit the Weibull distribution.

decrease the longitudinal strength of the 0° plies by about 5% (if the fraction of 0° vs. 90° plies is 50/50), and increase the fibre break density near the transverse crack tip [87]. However, in reality, transverse cracks occur early on and are often accompanied by delaminations, both lowering the effect they may have on fibre break development in the 0° plies. No increased fibre break density was observed in the vicinity of the 0/90 ply interfaces nor near transverse cracks. These observations agree with the work of Scott et al. [56]. Furthermore, a later paper by Scott et al. [43] confirmed that including transverse cracks and splits reduced the predicted longitudinal tensile strength of the 0° plies by just a few percent.

- Similarly, the effect of the notch is removed through the occurrence of splits at low load levels: at 55–65% and 40–50% of the failure load for 34–700 and T700SC, respectively. No preferential fibre break or cluster development in the central region of the notch was observed (see Fig. 3).
- Unpublished FE models from KU Leuven confirmed that the expected stress non-uniformity over the imaged region due to the notch and transverse cracks is limited. However, some stress concentrations do arise at the tips of the splits and delaminations. This is likely why the SRCT specimens tend to fail 1–2 mm away from the notched region. Fibre break and cluster development can thus be measured reliably, but failure may have occurred slightly prematurely. Some caution is, therefore, warranted in interpreting the fibre break and cluster parameters at failure.

3PFM, DFBM, DYSEM and FEISM overpredict significantly the failure strain and strength (see Fig. 7 and Fig. 8), whereas ABS and HSL are relatively close to the experimental results. For HSL, this difference is attributed to two conservative features: stress concentrations of 100% in nearby fibres, which are significantly higher than those predicted by other models for single fibre breaks or 2-plets (see Fig. 6b and d), and the fact that it imposes coplanarity once breaks have occurred. Both features resulted in cluster development being predicted at lower stresses and subsequent failure at lower stresses than 3PFM, DFBM, DYSEM and FEISM. For ABS, this difference is attributed to two features: (1) stress concentrations on the nearest neighbours are assumed constant over an axial length of 500 μm (see Fig. 6b), whereas they decrease rapidly with distance for the other models, and (2) the discarding of strength values larger than two standard deviations above the mean.

The fibre break density evolutions were not predicted well (see Fig. 10). This mismatch could be related to the uncertainty in the measured Weibull distribution. HSL was therefore used to predict fibre break density evolution for the extremes of the 95% confidence limits on the measured Weibull distribution, as provided by Matlab's '*wblfit*' function. This implied that the Weibull scale parameter σ_0 was set to 4120 ('low σ_0') or 4492 ("high σ_0") MPa, and the Weibull modulus m to 4.4 ('low m') or 6.1 ('high m') rather than the 4306 ('nominal σ_0') MPa and 5.1 ('nominal m') as reported in Table 5.

Fig. 14 reveals significant changes if the extremes of the distribution are used as input. However, the fibre break density evolution is still overpredicted, even for the best-case scenario (high m and high σ_0). This fibre break density overprediction occurs even for low applied stresses, where predicted fibre break density evolutions are governed by the Weibull parameters, as demonstrated in Fig. 10. Consequently, we would expect that all models included in this benchmark (apart from ABS) would predict similar bounds for the predicted fibre break density as those shown in Fig. 14 (at least up to 2000 MPa). Therefore, this mismatch between models and experiments suggests that the Weibull fibre strength distribution assumed in the models is not the same as the actual strength distribution of the fibres *in situ*, and that this difference

cannot be due to statistical uncertainty of the single fibre tensile testing data (as shown by the analysis in Fig. 14). The single fibre tensile testing data hence seems insufficient to represent accurately the actual strength distribution of the fibres within the composite, despite testing a large number of fibres (89 and 92).

We therefore also fitted a Weibull distribution to all individual fibre breaks in the first 34–700 specimen. The procedure has been thoroughly described in [88], and resulted in a Weibull scale parameter σ_0 of 5566 MPa and a Weibull shape parameter of 6.05 at a reference gauge length of 12 mm. Using the new distribution, the predicted strengths increased by 16–19%, bringing HSL closer to the experimental strength values, and 3PFM, DFBM and FEISM further away (see Fig. 15a). An excellent fit for the fibre break density was obtained for 3PFM, FEISM and HSL (see Fig. 15b), which validates the accuracy of the fitting procedure. The predictions for the 2-plet + 3-plet density (see Fig. 15c) also improved considerably for both models. The predictions for the largest cluster size deteriorated for 3PFM and FEISM but improved for HSL (see Fig. 15d).

The exact reason for the discrepancies in Fig. 14 and Fig. 15 remains unclear at present, but we can formulate several hypotheses:

- The single fibre tensile tests were performed at a gauge length of 12 mm, while the fibre break density in the microscale specimens was measured over a length of less than 2 mm. The assumed Weibull length scaling is perhaps not correct, and other Weibull-like distributions should be considered, as suggested by some authors [4–6,9].
- The carbon fibres may have an increased apparent strength when present in a matrix (e.g. due to a protective effect of the matrix with respect to surface flaws in the fibres); however, this remains unproven for carbon fibres, and other authors [80] have reported similar strengths measured with single-fibre tests and with single-fibre fragmentation tests (in which the fibres are impregnated by a matrix).
- The single fibre tensile tests may underestimate the fibre strength due to a range of issues, such as fibre misalignment and stress concentrations at the glue in the specimen holder [13,15]. However, we note that the single fibre tensile tests were carefully executed using a highly automated procedure and plastic tabs that avoid fibre misalignment (see [89]).

The results of Fig. 14 and Fig. 15 show that these hypotheses warrant further investigation.

The three models that have the most detailed approach to capturing the stress redistribution around fibre breaks (3PFM, DYSEM and FEISM) are also the ones that predicted excessively high 2-plet, 3-plet development and largest cluster sizes for both Weibull fibre strength distributions considered in Fig. 14 and Fig. 15. An increased length over which SCFs are significant in the nearby fibres, as is the case for ABS, or increased stress concentrations in nearby fibres, as is the case for HSL, lead to more accurate predictions for those parameters. However, the physical reasons behind such conservative assumptions should be carefully evaluated:

- The presence of debonding is known to promote longer ineffective lengths that are consistent with the ABS assumption. In the present work, the models included shear yielding of the matrix or interface, but ignored debonding (as instructed). However, Schöberl et al. [51] showed that debonding was either absent or very limited, as strain recovery occurred over a distance of about 63 μm at an applied strain of 1.5%. The material used by Schöberl et al. is almost identical to the T700SC composite used here, apart from the hardener being KTA313 instead of KTA315. This information was, however, not available when the benchmarking exercise started.
- Longer ineffective lengths and higher stress concentrations could in turn be associated to matrix microcracking around the fibre breaks, given the high local shear strains. However, epoxy resins are known to behave in a much more ductile manner and to have an increase in apparent strength at the microscale than in large neat resin specimens [36]. Therefore, it remains unclear whether incorporating microscale properties would result in increased stress concentrations or increased stress recovery lengths.
- Dynamic stress concentrations are temporarily higher than the static ones and are generally acknowledged to occur in reality. However, DYSEM does capture this feature, and has already shown that the effect on strength predictions is limited [32].
- All models assume uniform stress concentrations over the entire fibre cross-section, even though the local values are much higher. Yamamoto et al. [90] recently performed experimental work indicating that these local stress concentrations can be about twice as high as the averaged stress concentrations. FE models even indicated that they may be up to seven times higher, albeit in a very small volume [2]. From a fracture mechanics point of view, the role of individual breaks or clusters might be better described by a stress intensity factor to characterise a singular stress field, particularly with large clusters; including a fracture mechanics-based criterion could thus improve the ability to replicate experimental data [91]. The treatment of stress redistributions is therefore the most likely root cause for the underestimation of SCFs.

Another hypothesis to explain the excessively high 2-plet, 3-plet development and largest cluster sizes, is that the strength of fibres is somewhat dependent on their location in the composite, an effect that is not captured by any Weibull distribution. Such spatial dependency could be due to (1) fluctuations in carbon fibre production conditions creating adjacent fibres that are weaker in the same axial location or (2) damage introduced during prepreg manufacturing. Both hypotheses are difficult to prove, but they are worth further investigation. It is, however, clear that the prepreg manufacturing did not cause fibre breakage, as such breaks would have been spotted in the initial volumes.

3PFM, DYSEM and FEISM predict a much lower coplanarity than experimentally observed (see Fig. 13). It seems consistent that these models are also the ones with the most significant overpredictions of failure strain and strength (see Fig. 7 and Fig. 8). In fact, coplanar clusters lead to higher stress concentrations in the nearby fibres than non-coplanar ones. It should be noted that several studies reported similar effects in microcomposites, in which fibre breaks were more likely to occur in a coplanar fashion than theoretical models would predict [90,92,93]. A thorough understanding of the reason for the coplanarity of clusters is, however, still lacking [2]. The reasons may be similar as the ones mentioned earlier for the overpredictions by 3PFM, DYSEM and FEISM: dynamic and local stress concentrations. Dynamic stress concentration effects could be contributing, as they decay sharply with axial distance. However, DYSEM incorporates these effects and still predicts coplanarity similar to 3PFM and FEISM (see Fig. 13). These effects are likely to be more significant for a linear elastic matrix, which would account for the lack of time for the polymer to respond to fast stress changes.

The local stress concentrations are more likely to cause this coplanarity, as they decay even more sharply with axial distance. Note that the experiments presented herein confirm that imposing coplanarity is also unrealistic, as the experiments still have a significant 3-plet height standard deviation (see Fig. 13). This aspect merits further attention from the community.

6. Conclusions

A detailed experimental validation was performed for blind predictions of six state-of-the-art strength models for longitudinal tensile failure. The experiments are the most detailed ones reported so far in the literature, and lead to several important conclusions:

- The difference between nominally identical microscale specimens was limited for failure strain, strength and fibre break density, but

was larger for parameters related to cluster development. Verifying the repeatability of the microscale specimens is, therefore, vital, despite the fact that they involve a large number of fibres in the cross-section. The analysis of specimen-to-specimen variability was, however, encouraging, as models predict similar levels of variability for most parameters.
- When differences in size and V_f are considered, the microscale strength values were reasonably in line with the macroscale strength. This proves the minor influence of the notch and 90° plies.

The comparison of model predictions with the detailed SRCT microscale experiments enabled us to draw the following conclusions:

- ABS and HSL were able to predict strength and failure strain reasonably well, while the other four models overpredicted them. This difference is mainly due to larger stress recovery length, higher stress concentrations on the nearby fibres and imposed cluster coplanarity of ABS and HSL.
- All models overpredicted the fibre break density observed in the experiments, suggesting that it is vital to improve methods to accurately characterise the strength distribution of fibres in the composite.
- Apart from HSL, all models overpredicted the non-linearity of the stress–strain diagram primarily due to overpredicting the fibre break density at failure. For fibre break densities close to the experimental density at failure, however, all the models predict the non-linearity well.
- After fitting a unimodal Weibull distribution to the fibre break density observed in the experiments, 3PFM, FEISM and HSL predicted the fibre break density accurately. This improved the agreement between predictions and experiments in some models and for some parameters but worsened in others.
- The models capable of capturing cluster coplanarity (3PFM, DYSEM and FEISM) predict a much lower coplanarity than experimentally observed. Imposing coplanarity, however, as done by ABS and HSL, also does not capture the non-coplanarity of the clusters observed experimentally.

The instructions for this benchmarking exercise and all necessary input parameters are publicly available [72], and the experimental results can be obtained from the accompanying *Data in Brief* article [63]. It is our aspiration that this data set and paper will: (1) become a benchmark for new models, and (2) inspire researchers to develop improved models and refined experimental methods. The ability to predict tensile strength and its statistics accurately from fibre, matrix and interface properties is a key goal for the composite materials modelling community, and a key requirement to develop future generations of materials with superior properties.

CRediT authorship contribution statement

C. Breite: Conceptualization, Methodology, Software, Formal analysis, Investigation, Writing – review & editing. **A. Melnikov:** Conceptualization, Methodology, Software, Formal analysis, Investigation, Writing – review & editing. **A. Turon:** Writing – review & editing, Supervision. **A.B. de Morais:** Software, Investigation, Writing – review & editing. **C. Le Bourlot:** Methodology, Investigation, Writing – review & editing. **E. Maire:** Methodology, Investigation, Writing – review & editing. **E. Schöberl:** Conceptualization, Methodology, Investigation, Writing – review & editing. **F. Otero:** Software, Writing – review & editing. **F. Mesquita:** Conceptualization, Methodology, Software, Investigation, Writing – review & editing. **I. Sinclair:** Conceptualization, Methodology, Investigation, Writing – review & editing, Supervision. **J. Costa:** Writing – review & editing, Supervision. **J.A. Mayugo:** Writing – review & editing, Supervision. **J.M. Guerrero:** Writing – review & editing, Software, Investigation. **L. Gorbatikh:** Writing – review & editing, Supervision. **L.N. McCartney:** Writing – review & editing, Software, Investigation. **M. Hajikazemi:** Writing – review & editing, Software, Investigation. **M. Mehdikhani:** Formal analysis, Investigation, Writing – review & editing. **M.N. Mavrogordato:** Writing – review & editing, Supervision, Methodology. **P.P. Camanho:** Writing – review & editing, Supervision. **R. Tavares:** Writing – review & editing, Software, Investigation. **S.M. Spearing:** Conceptualization, Methodology, Investigation, Writing – review & editing, Supervision. **S.V. Lomov:** Writing – review & editing, Supervision. **S. Pimenta:** Conceptualization, Methodology, Software, Investigation, Writing – review & editing. **W. Van Paepegem:** Investigation, Writing – review & editing, Supervision. **Y. Swolfs:** Conceptualization, Methodology, Software, Formal analysis, Investigation, Writing – review & editing, Visualization, Supervision.

Declaration of Competing Interest

The authors declare that they have no known competing financial interests or personal relationships that could have appeared to influence the work reported in this paper.

Acknowledgements

The research leading to these results has been conducted in the framework of the FiBreMoD project and has received funding from the European Union's Horizon 2020 research and innovation programme under the Marie Skłodowska-Curie grant agreement No. 722626. Compressive tests on the neat epoxy resin were performed at the mechanical lab of the Institute of Mechanics, Materials and Civil Engineering (IMMC), Université Catholique de Louvain (UCLouvain) with the kind support of J. Chevalier and T. Pardoen. M.J. Emerson from QIM, Technical University of Denmark (DTU) is thankfully acknowledged for the hands-on training sessions and support of the Insegt Fibre segmentation toolbox. Support of C. Schlepütz from TOMCAT beamline at Swiss Light Source for optimising the acquisition settings during the beamtimes under proposal IDs 20161157 and 20171494 is thankfully acknowledged. J.M. Guerrero would like to acknowledge the grant BES-2016-078270 from the 'Subprograma Estatal de Formación del MICINN' co-financed by the European Social Fund, and all authors from the University of Girona acknowledge the funding from the Spanish project RTI2018-097880-B-I00. The work of M. Hajikazemi forms part of the research programme of DPI, project 812 T17. S. Pimenta acknowledges the funding from the Royal Academy of Engineering in the scope of her Research Fellowship on "Multiscale discontinuous composites for high-volume and sustainable applications" (2015-2019). R.P. Tavares and P. P. Camanho would like to thank the financial support provided by FCT - Fundação para a Ciência e a Tecnologia through National Funds in the scope of project MITP-TB/PFM/0005/2013. The authors would also like to thank A.R. Bunsell, S. Joannès, J. Rojek and A. Thionnet for their help in setting up the instructions.

References

[1] Huang Z-M. On micromechanics approach to stiffness and strength of unidirectional composites. J Reinf Plast Compos. 2019;38(4):167–96.
[2] Swolfs Y, Verpoest I, Gorbatikh L. A review of input data and modelling assumptions in longitudinal strength models for unidirectional fibre-reinforced composites. Compos Struct. 2016;150:153–72.
[3] Curtin WA. Stochastic damage evolution and failure in fiber-reinforced composites. Adv Appl Mech 1998;36(36):163–253.
[4] Watanabe J, Tanaka F, Okuda H, Okabe T. Tensile strength distribution of carbon fibers at short gauge lengths. Adv Compos Mater. 2014;23(5–6):535–50.
[5] Watson AS, Smith RL. An examination of statistical theories for fibrous materials in the light of experimental data. J Mater Sci. 1985;20(9):3260–70.
[6] Okabe T, Takeda N. Size effect on tensile strength of unidirectional CFRP composites - experiment and simulation. Compos Sci Technol. 2002;62(15):2053–64.
[7] Beyerlein IJ, Phoenix SL. Statistics for the strength and size effects of microcomposites with four carbon fibers in epoxy resin. Compos Sci Technol. 1996;56(1):75–92.

[8] Gulino R, Phoenix SL. Weibull strength statistics for graphite fibres measured from the break progression in a model graphite/glass/epoxy composite. J Mater Sci. 1991;26(11):3107–18.
[9] Curtin WA. Tensile strength of fiber-reinforced composites: III. Beyond the traditional Weibull model for fiber strengths. J Compos Mater. 2000;34(15):1301–32.
[10] Swolfs Y, Verpoest I, Gorbatikh L. Issues in strength models for unidirectional fibre-reinforced composites related to Weibull distributions, fibre packings and boundary effects. Compos Sci Technol. 2015;114:42–9.
[11] Berger MH, Jeulin D. Statistical analysis of the failure stresses of ceramic fibres: Dependence of the Weibull parameters on the gauge length, diameter variation and fluctuation of defect density. J Mater Sci. 2003;38(13):2913–23.
[12] Islam F, Joannès S, Bucknell S, Leray Y, Bunsell A, Laiarinandrasana L. Investigation of tensile strength and dimensional variation of T700 carbon fibres using an improved experimental setup. J Reinf Plast Compos. 2020;39(3–4):144–62.
[13] Islam F, Joannès S, Laiarinandrasana L. Evaluation of Critical Parameters in Tensile Strength Measurement of Single Fibres. J Compos Sci. 2019;3(3):69.
[14] Joannès S, Islam F, Laiarinandrasana L. Uncertainty in fibre strength characterisation due to uncertainty in measurement and sampling randomness. Appl Compos Mater. 2020;27:165–84.
[15] Stoner EG, Edie DD, Durham SD. An end-effect model for the single-filament tensile test. J Mater Sci. 1994;29(24):6561–74.
[16] Swolfs Y, Morton H, Scott AE, Gorbatikh L, Reed PAS, Sinclair I, et al. Synchrotron radiation computed tomography for experimental validation of a tensile strength model for unidirectional fibre-reinforced composites. Compos Part A Appl Sci Manuf. 2015;77:106–13.
[17] Hedgepeth JM. *Stress concentrations in filamentary structures*. NASA TN. 1961;D-882 1-36.
[18] Hedgepeth JM, Van Dyke P. Local stress concentrations in imperfect filamentary composite materials. J Compos Mater. 1967;1(3):294–309.
[19] Landis CM, McGlockton MA, McMeeking RM. An improved shear lag model for broken fibers in composite materials. J Compos Mater. 1999;33(7):667–80.
[20] Beyerlein IJ, Phoenix SL. Stress concentrations around multiple fiber breaks in an elastic matrix with local yielding or debonding using quadratic influence superposition. J Mech Phys Solids. 1996;44(12):1997–2039.
[21] Zhou SJ, Curtin WA. Failure of fiber composites: a lattice green function model. Acta Metall Mater. 1995;43(8):3093–104.
[22] Nedele MR, Wisnom MR. Three-dimensional finite element analysis of the stress concentration at a single fibre break. Compos Sci Technol. 1994;51(4):517–24.
[23] Xia Z, Okabe T, Curtin WA. Shear-lag versus finite element models for stress transfer in fiber-reinforced composites. Compos Sci Technol. 2002;62(9):1141–9.
[24] Swolfs Y, Gorbatikh L, Romanov V, Orlova S, Lomov SV, Verpoest I. Stress concentrations in an impregnated fibre bundle with random fibre packing. Compos Sci Technol. 2013;74:113–20.
[25] Swolfs Y, McMeeking RM, Verpoest I, Gorbatikh L. Matrix cracks around fibre breaks and their effect on stress redistribution and failure development in unidirectional composites. Compos Sci Technol. 2015;108:16–22.
[26] van den Heuvel PWJ, Goutianos S, Young RJ, Peijs T. Failure phenomena in fibre-reinforced composites. Part 6: a finite element study of stress concentrations in unidirectional carbon fibre-reinforced epoxy composites. Compos Sci Technol. 2004;64(5):645–56.
[27] van den Heuvel PWJ, Wubbolts MK, Young RJ, Peijs T. Failure phenomena in two-dimensional multi-fibre model composites: 5. A finite element study. Compos Part A Appl Sci Manuf. 1998;29(9–10):1121–35.
[28] Blassiau S, Thionnet A, Bunsell AR. Micromechanisms of load transfer in a unidirectional carbon fibre-reinforced epoxy composite due to fibre failures. Part 2: Influence of viscoelastic and plastic matrices on the mechanisms of load transfer. Compos Struct. 2006;74(3):319–31.
[29] St-Pierre L, Martorell NJ, Pinho ST. Stress redistribution around clusters of broken fibres in a composite. Compos Struct. 2017;168:226–33.
[30] Swolfs Y, Gorbatikh L, Verpoest I. Stress concentrations in hybrid unidirectional fibre-reinforced composites with random fibre packings. Compos Sci Technol. 2013;85:10–6.
[31] Okabe T, Sekine H, Ishii K, Nishikawa M, Takeda N. Numerical method for failure simulation of unidirectional fiber-reinforced composites with spring element model. Compos Sci Technol. 2005;65(6):921–33.
[32] Tavares RP, Otero F, Baiges J, Turon A, Camanho pp.. A dynamic spring element model for the prediction of longitudinal failure of polymer composites. Comput Mater Sci. 2019;160:42–52.
[33] Tavares RP, Otero F, Turon A, Camanho pp.. Effective simulation of the mechanics of longitudinal tensile failure of unidirectional polymer composites. Int J Fract. 2017;208:269–85.
[34] Okabe T, Ishii K, Nishikawa M, Takeda N. Prediction of Tensile Strength of Unidirectional CFRP Composites. Adv Compos Mater. 2010;19(3):229–41.
[35] Pimenta S, Pinho ST. Hierarchical scaling law for the strength of composite fibre bundles. J Mech Phys Solids. 2013;61(6):1337–56.
[36] Sui XM, Tiwari M, Greenfeld I, Khalfin RL, Meeuw H, Fiedler B, et al. Extreme scale-dependent tensile properties of epoxy fibers. Express Polym Lett. 2019;13:993–1003.
[37] McCartney LN. *Simulation of progressive fiber failure during the tensile loading of unidirectional composites*. NPL report CMMT(A)212: National Physical Laboratory. UK 1999.
[38] Zhao FM, Takeda N. Effect of interfacial adhesion and statistical fiber strength on tensile strength of unidirectional glass fiber/epoxy composites. Part. II: comparison with prediction. Compos Part A Appl Sci Manuf. 2000;31(11):1215–24.
[39] Guerrero JM, Mayugo JA, Costa J, Turon A. Failure of hybrid composites under longitudinal tension: Influence of dynamic effects and thermal residual stresses. Compos Struct. 2020;233:111732.
[40] Guerrero JM, Mayugo JA, Costa J, Turon A. A 3D Progressive Failure Model for predicting pseudo-ductility in hybrid unidirectional composite materials under fibre tensile loading. Compos Part A Appl Sci Manuf. 2018;107:579–91.
[41] Paipetis A, Galiotis C, Liu YC, Nairn JA. Stress transfer from the matrix to the fibre in a fragmentation test: Raman experiments and analytical modeling. J Compos Mater. 1999;33(4):377–99.
[42] Bunsell A, Gorbatikh L, Morton H, Pimenta S, Sinclair I, Spearing M, et al. Benchmarking of strength models for unidirectional composites under longitudinal tension. Compos Part A Appl Sci Manuf. 2018;111:138–50.
[43] Scott AE, Sinclair I, Spearing SM, Thionnet A, Bunsell AR. Damage accumulation in a carbon/epoxy composite: Comparison between a multiscale model and computed tomography experimental results. Compos Part A Appl Sci Manuf. 2012;43(9):1514–22.
[44] Garcea SC, Mavrogordato MN, Scott AE, Sinclair I, Spearing SM. Fatigue micromechanism characterisation in carbon fibre reinforced polymers using synchrotron radiation computed tomography. Compos Sci Technol. 2014;99:23–30.
[45] Garcea SC, Sinclair I, Spearing SM. In situ synchrotron tomographic evaluation of the effect of toughening strategies on fatigue micromechanisms in carbon fibre reinforced polymers. Compos Sci Technol. 2015;109:32–9.
[46] Aroush DRB, Maire E, Gauthier C, Youssef S, Cloetens P, Wagner HD. A study of fracture of unidirectional composites using in situ high-resolution synchrotron X-ray microtomography. Compos Sci Technol. 2006;66(10):1348–53.
[47] Wright P, Fu X, Sinclair I, Spearing SM. Ultra high resolution computed tomography of damage in notched carbon fiber-epoxy composites. J Compos Mater. 2008;42(19):1993–2002.
[48] Garcea SC, Sinclair I, Spearing SM, Withers PJ. Mapping fibre failure in situ in carbon fibre reinforced polymers by fast synchrotron X-ray computed tomography. Compos Sci Technol. 2017;149:81–9.
[49] Schöberl E, Breite C, Rosini S, Swolfs Y, Mavrogordato MN, Sinclair I, et al. A novel particle-filled Carbon-Fibre Reinforced Polymer model composite tailored for the application of Digital Volume Correlation and Computed Tomography. J Compos Mater. 2021;55(14):1907–34.
[50] Rosini S, Mavrogordato MN, Egorova O, Matthews ES, Jackson SE, Mark Spearing S, et al. In situ statistical measurement of local morphology in carbon-epoxy composites using synchrotron X-ray computed tomography. Compos Part A Appl Sci Manuf. 2019;125:105543.
[51] Schöberl E, Breite C, Melnikov A, Swolfs Y, Mavrogordato MN, Sinclair I, et al. Fibre-direction strain measurement in a composite ply under quasi-static tensile loading using Digital Volume Correlation and in situ Synchrotron Radiation Computed Tomography. Compos Part A Appl Sci Manuf. 2020;137:105935.
[52] Schöberl E, Mavrogordato MN, Sinclair I, Spearing SM. Fibre direction strain measurement in a composite ply under pure bending using Digital Volume Correlation and Micro-focus Computed Tomography. J Compos Mater. 2020;54(14):1889–912.
[53] Mehdikhani M, Breite C, Swolfs Y, Soete J, Wevers M, Lomov SV, et al. Digital volume correlation for meso/micro in-situ damage analysis in carbon fiber reinforced composites. Compos Sci Technol. 2021;213:108944.
[54] Pimenta S. A computationally-efficient hierarchical scaling law to predict damage accumulation in composite fibre-bundles. Compos Sci Technol. 2017;146:210–25.
[55] Wright P, Moffat A, Sinclair I, Spearing SM. High resolution tomographic imaging and modelling of notch tip damage in a laminated composite. Compos Sci Technol. 2010;70(10):1444–52.
[56] Moffat AJ, Wright P, Buffière JY, Sinclair I, Spearing SM. Micromechanisms of damage in 0° splits in a [90/0]s composite material using synchrotron radiation computed tomography. Scripta Mater. 2008;59(10):1043–6.
[57] Scott AE, Mavrogordato M, Wright P, Sinclair I, Spearing SM. In situ fibre fracture measurement in carbon-epoxy laminates using high resolution computed tomography. Compos Sci Technol. 2011;71:1471–7.
[58] Czél G, Jalalvand M, Wisnom MR. Hybrid specimens eliminating stress concentrations in tensile and compressive testing of unidirectional composites. Compos Part A Appl Sci Manuf. 2016;91:436–47.
[59] Wisnom MR, Czel G, Swolfs Y, Jalalvand M, Gorbatikh L, Verpoest I. Hybrid effects in thin ply carbon/glass unidirectional laminates: accurate experimental determination and prediction. Compos Part A Appl Sci Manuf. 2016;88:131–9.
[60] SiPreg Technical Datasheet, SR8500, KTA 31x,. Sicomin. France: Châteauneuf les Martigues; 2014.
[61] ThinPreg NTPT, 736LT Data sheet,. North Thin Ply Technology. Switzerland: Renens; 2017.
[62] Schapery RA. Thermal Expansion Coefficients of Composite Materials Based on Energy Principles. J Compos Mater. 1968;2(3):380.
[63] Breite C, Melnikov A, Turon A, de Morais AB, Le Bourlot C, Maire E, et al. *Dataset for second international benchmarking exercise on longitudinal tensile failure of unidirectional composites*. Data in Brief, in press.
[64] Maire E, Le Bourlot C, Adrien J, Mortensen A, Mokso R. 20 Hz X-ray tomography during an in situ tensile test. Int J Fract. 2016;200(1):3–12.
[65] Mokso R, Schleputz CM, Theidel G, Billich H, Schmid E, Celcer T, et al. GigaFRoST: the gigabit fast readout system for tomography. J Synchrotron Radiat. 2017;24(6):1250–9.

[66] Straumit I, Lomov SV, Wevers M. Quantification of the internal structure and automatic generation of voxel models of textile composites from X-ray computed tomography data. Compos Part A Appl Sci Manuf. 2015;69:150–8.

[67] Batdorf SB. Tensile Strength of Unidirectionally Reinforced Composites — I. J Reinf Plast Compos. 1982;1(2):153–64.

[68] Schindelin J, Arganda-Carreras I, Frise E, Kaynig V, Longair M, Pietzsch T, et al. Fiji: an open-source platform for biological-image analysis. Nat Methods. 2012;9(7):676–82.

[69] Emerson MJ, Jespersen KM, Dahl AB, Conradsen K, Mikkelsen LP. Individual fibre segmentation from 3D X-ray computed tomography for characterising the fibre orientation in unidirectional composite materials. Compos Part A Appl Sci Manuf. 2017;97:83–92.

[70] Breite C, Melnikov A, Turon A, de Morais AB, Otero F, Mesquita F, et al. Blind benchmarking of seven longitudinal tensile failure models for two virtual unidirectional composites. Compos Sci Technol. 2021;202:108555.

[71] Mesquita F, Swolfs Y, Bucknell S, Leray Y, Lomov SV, Gorbatikh L. Tensile properties of single carbon fibres tested with automated equipment. 22nd International Conference on Composite Materials. 2019.

[72] Breite C, Gorbatikh L, Swolfs Y, Alves M, Pimenta S, Schöberl E, et al., *Benchmarking exercise II for longitudinal strength models of unidirectional composites - Instructions for participants, www.fibremodproject.eu*, FiBreMoD European Training Network, June 2020.

[73] Searles K, Odegard G, Kumosa M. Micro- and mesomechanics of 8-harness satin woven fabric composites: I - evaluation of elastic behavior. Compos Part A Appl Sci Manuf. 2001;32(11):1627–55.

[74] Shindo A. Polyacrylonitrile (PAN)-based carbon fibers. In: Kelly A, Zweben C, Chou TW, editors. Comprehensive composite materials, vol. 1.01. Amsterdam: Elsevier; 2000. p. 1–33.

[75] Kulkarni R, Ochoa O. Transverse and longitudinal CTE measurements of carbon fibers and their impact on interfacial residual stresses in composites. J Compos Mater. 2006;40(8):733–54.

[76] Motoc DL, Ivens J, Dadirlat N. Coefficient of thermal expansion evolution for cryogenic preconditioned hybrid carbon fiber/glass fiber-reinforced polymeric composite materials. J Therm Anal Calorim. 2013;112(3):1245–51.

[77] Hartman DR, Greenwood ME, Miller DM. High strength glass fibres. AGY Technical Paper: Owens Corning Corp; 1996.

[78] Durai Prabhakaran RT, Andersen TL, Markussen CM, Madsen B, Lilholt H. *Tensile and compression properties of hybrid composites – A comparative study*. 19th International Conference on Composite Materials, Montréal, Canada 2013.

[79] Morelle XP, Chevalier J, Bailly C, Pardoen T, Lani F. Mechanical characterization and modeling of the deformation and failure of the highly crosslinked RTM6 epoxy resin. Mech Time-Depend Mater. 2017;21(3):419–54.

[80] Tanaka F, Okabe T, Okuda H, Kinloch IA, Young RJ. Factors Controlling the Strength of Carbon Fibres in Tension. Compos Part A Appl Sci Manuf. 2014;57:88–94.

[81] Kant M, Penumadu D. Dynamic mechanical characterization for nonlinear behavior of single carbon fibers. Compos Part A Appl Sci Manuf. 2014;66:201–8.

[82] Beetz CP. Strain-induced stiffening of carbon fibres. Fibre Sci Technol. 1982;16(3):219–29.

[83] Hughes JDH. Strength and modulus of current carbon fibres. Carbon 1986;24(5):551–6.

[84] Curtis GJ, Milne JM, Reynolds WN. Non-Hookean Behaviour of Strong Carbon Fibres. Nature 1968;220(5171):1024–5.

[85] Wisnom MR, Khan B, Hallett SR. Size effects in unnotched tensile strength of unidirectional and quasi-isotropic carbon/epoxy composites. Compos Struct. 2008;84(1):21–8.

[86] McCartney LN. Physically based damage models for laminated composites. Proc Inst Mech Eng L. 2003;217(3):163–99.

[87] Melnikov A, Swolfs Y, Lomov SV, Gorbatikh L. *Influence of transverse cracking on strength and fibre break development in cross-ply laminates*. 7th ECCOMAS Thematic Conference on the Mechanical Response of Composites, Girona, Spain, 2019.

[88] Mesquita F. *Unidirectional interply fibre-hybrid composites: longitudinal tensile failure and interactions between fibre types* PhD thesis. KU Leuven. Materials Engineering 2020.

[89] Mesquita F, Bucknell S, Leray D, Lomov SV, Swolfs Y. Single carbon and glass fibre properties characterised using large data sets obtained through automated single fibre tensile testing. Compos Part A Appl Sci Manuf. 2021;145:106389.

[90] Yamamoto G, Onodera M, Koizumi K, Watanabe J, Okuda H, Tanaka F, et al. Considering the stress concentration of fiber surfaces in the prediction of the tensile strength of unidirectional carbon fiber-reinforced plastic composites. Compos Part A Appl Sci Manuf. 2019;121:499–509.

[91] Bullegas G, Moledo Lamela J, Pimenta S, Taveira Pinho S. On the role of dynamic stress concentrations and fracture mechanics in the longitudinal tensile failure of fibre-reinforced composites. Eng Fract Mech. 2020;228:106920.

[92] Watanabe J, Tanaka F, Higuchi R, Matsutani H, Okuda H, Okabe T. A study of stress concentrations around fiber breaks in unidirectional CF/epoxy composites using double-fiber fragmentation tests. Adv Compos Mater. 2018;27(6):575–87.

[93] van den Heuvel PWJ, vanderBruggen YJW, Peijs T.. Failure phenomena in multi-fibre model composites.1. An experimental investigation into the influence of fibre spacing and fibre-matrix adhesion. Compos Part A Appl Sci Manuf. 1996;27(9):855–9.

[94] Guerrero JM, Tavares RP, Otero F, Mayugo JA, Costa J, Turon A, et al. An analytical model to predict stress fields around broken fibres and their effect on the longitudinal failure of hybrid composites. Compos Struct. 2019;211:564–76.

[95] McCartney LN. Analytical Models for Sliding Interfaces Associated with Fibre Fractures or Matrix Cracks. Comput Mater Contin. 2013;35(3):183–227.

[96] de Morais AB. Prediction of the longitudinal tensile strength of polymer matrix composites. Compos Sci Technol. 2006;66(15):2990–6.

[97] Tavares RP, Melro AR, Bessa MA, Turon A, Liu WK, Camanho pp.. Mechanics of hybrid polymer composites: analytical and computational study. Comput Mech. 2016;57:405–21.

[98] Swolfs Y, Verpoest I, Gorbatikh L. Maximising the hybrid effect in unidirectional hybrid composites. Mater Des. 2016;93:39–45.

[99] Swolfs Y, Fazlali B, Melnikov A, Mesquita F, Feyen V, Breite C, et al. State-of-the-art models for mechanical performance of carbon-glass hybrid composites in wind turbine blades. IOP Conf Ser Mat Sci Eng. 2020;942:012005.

[100] Mesquita F, Swolfs Y, Lomov SV, Gorbatikh L. Ply fragmentation in unidirectional hybrid composites linked to stochastic fibre behaviour: A dual-scale model. Compos Sci Technol. 2019;181:107702.